

## Constraining Star Formation Histories of Blue Galaxies using the Scatter between Stellar Mass and Halo Mass

CHANGHOON HAHN,<sup>1,2,3,\*</sup> JEREMY L. TINKER,<sup>3</sup> AND ANDREW WETZEL<sup>4</sup>

<sup>1</sup>*Lawrence Berkeley National Laboratory, 1 Cyclotron Rd, Berkeley CA 94720, USA*

<sup>2</sup>*Berkeley Center for Cosmological Physics, University of California, Berkeley, CA 94720, USA*

<sup>3</sup>*Center for Cosmology and Particle Physics, Department of Physics, New York University, 4 Washington Place, New York, NY 10003*

<sup>4</sup>*Department of Physics, University of California, Davis, CA USA*

### ABSTRACT

We present constraints on the timescale of star formation variability and the correlation between star formation and host halo accretion histories of star-forming (SF) central galaxies from the measured scatter of the stellar-to-halo mass relation (SHMR). SF galaxies are found to have a tight relationship between their star formation rates and stellar masses on the so-called “star-forming sequence” (SFS), which characterizes both their star formation histories and stellar mass growths. Meanwhile, observed constraints on the SHMR connect stellar mass growth to host halo accretion history. Combining these observed trends with a cosmological  $N$ -body simulation, we present flexible models that track the star formation, stellar mass, and host halo accretion histories of SF central galaxies at  $z < 1$  while reproducing the observed stellar mass function and SFS of central galaxies in SDSS Data Release 7. Using these models, we find that the scatter in SHMR at  $M_h = 10^{12} M_\odot$ ,  $\sigma_{M_*|M_h=10^{12} M_\odot}$ , is sensitive to the timescale of star formation variability,  $t_{\text{duty}}$ , and the correlation coefficient,  $r$ , between star formation and host halo accretion histories: shorter  $t_{\text{duty}}$  and higher  $r$  both result in tighter  $\sigma_{M_*|M_h=10^{12} M_\odot}$ . To reproduce a constant  $\sigma_{M_*|M_h} \sim 0.2$  dex over  $z = 1$  to 0, our models require  $t_{\text{duty}} \leq 1.5$  Gyr for  $r = 0.99$  or  $r > 0.6$  for  $t_{\text{duty}} = 0.1$  Gyr. For  $r \sim 0.6$ , as found in the literature,  $t_{\text{duty}} < 0.2$  Gyr is necessary. Meanwhile, to reproduce the tightening of  $\sigma_{M_*|M_h=10^{12} M_\odot} = 0.35$  to 0.2 dex from  $z = 1$  to 0 in hydrodynamical simulations, our models require  $t_{\text{duty}} = 0.1$  Gyr for  $r > 0.5$ . Although, the lack of consensus on  $\sigma_{M_*|M_h}$  at  $M_h = 10^{12} M_\odot$  and at  $z = 1$  from observations and galaxy formation models remains the main bottleneck in precisely constraining  $r$  and  $t_{\text{duty}}$ , we demonstrate that SHMR can be used to constrain star formation and host halo accretion histories of SF central galaxies.

*Keywords:* methods: numerical – galaxies: evolution – galaxies: haloes – galaxies: star formation – galaxies: groups: general – cosmology: observations.

## 1. INTRODUCTION

Observations from large surveys such as the Sloan Digital Sky Survey (SDSS; York et al. 2000) have been critical for establishing the global trends of galaxies in the local universe. Broadly speaking, galaxies fall into two categories: quiescent and star-forming (hereafter SF) galaxies. Quiescent galaxies have little to no star formation, are red in color due to old stellar populations, and have elliptical morphologies. Meanwhile, SF galaxies have significant star formation, thus are blue in color, and have disk-like morphologies (Kauffmann et al. 2003; Blanton et al. 2003; Baldry et al. 2006; Taylor et al. 2009; Moustakas et al. 2013; see Blanton & Moustakas 2009 and references therein). SF galaxies, furthermore, are found on the so-called “star-forming sequence” (hereafter SFS), a tight relationship between their star formation rates (SFR) and stellar masses (Noeske et al. 2007; Daddi et al. 2007; Salim et al. 2007; Speagle et al. 2014; Lee et al. 2015, see also Figure 1). This sequence, which is observed out to  $z > 2$  (Wang et al. 2013; Leja et al. 2015) plays a crucial role in determining galaxy evolution over the past  $\sim 10$  Gyr (see Kelson 2014; Abramson et al. 2016, for an alternative point of view). The significant fraction of SF galaxies that quench their star formation and migrate off of the SFS reflects the growth in the fraction of quiescent galaxies (Blanton 2006; Borch et al. 2006; Bundy et al. 2006; Moustakas et al. 2013). The decline of star formation in the entire SFS (Lee et al. 2015; Schreiber et al. 2015) over time reflects the decline in overall cosmic star formation (Hopkins & Beacom 2006; Behroozi et al. 2013; Madau & Dickinson 2014). With its evolution, the SFS also connects the star formation histories of SF galaxies to their stellar mass growths.

Recent observations have also allowed us to investigate how galaxies fit into the context of hierarchical structure formation predicted by  $\Lambda$ CDM cosmology. In addition to traditional theoretical models of hydrodynamic simulations and semi-analytic models (see Silk & Mamon 2012; Somerville & Davé 2015 for reviews), empirical models have been remarkably effective for understanding the galaxy-halo connection. These models relate galaxy properties to their host dark matter halo properties using methods such as halo occupation distribution modeling (HOD; *e.g.* Zheng et al. 2007; Zehavi et al. 2011; Leauthaud et al. 2012; Parejko et al. 2013; Zu & Mandelbaum 2015), conditional luminosity function modeling (*e.g.* Yang et al. 2009), and abundance matching (*e.g.* Kravtsov et al. 2004; Vale & Ostriker 2006; Conroy et al. 2009; Moster et al. 2013; Reddick et al. 2013). Using these models, more massive halos are found to host more massive galaxies on the stellar-to-halo mass relation (hereafter SHMR; Mandelbaum et al. 2006; Conroy et al. 2007; More et al. 2011; Leauthaud et al. 2012; Tinker et al. 2013; Velandar et al. 2014; Han et al. 2015; Zu & Mandelbaum 2015; Gu et al. 2016; Lange et al. 2018) with a tight scatter in  $\log M_*$  at fixed  $M_h$  —  $\sigma_{M_*|M_h}$  — of 0.2 dex. These constraints are mainly driven by massive halos with  $M_h > 10^{12} M_\odot$ . A similarly tight scatter is found at higher  $z \sim 1$  (Leauthaud et al. 2012; Tinker et al. 2013; Patel et al. 2015). The tight scatter in SHMR over  $z < 1$  suggests that stellar mass growth of galaxies is linked to the growth of their host dark matter halos.

Despite these developments, we face a number of challenges when it comes to understanding the detailed star formation histories (SFH) and its connection to host halo assembly history of galaxies.

\* hahn.changhoon@gmail.com

For instance, SFHs at lookback times longer than 200 Myr do not contribute to SFR indicators such as  $H\alpha$  or  $FUV$  fluxes (Sparre et al. 2017). Measuring SFHs from fitting photometry or spectroscopy typically assume a specific functional form of the SFH, such as exponentially declining or lognormal, that do not include variations on short timescales (*e.g.* Wilkinson et al. 2017; Carnall et al. 2018). Even methods that recover non-parametric SFHs from high signal-to-noise observations can only retrieve SFHs in coarse temporal resolutions (*e.g.* Tojeiro et al. 2009; Leja et al. 2018). While simulations provide another means for understanding SFHs, they are also subject to their specific time and mass resolutions that suppress the variability of their star formation, especially in analytic models, semi-analytic models, and large-volume cosmological hydrodynamic simulations (Sparre et al. 2017, see also Figure 2).

Empirical models, through their flexibility, provide an effective method for examining the connection between SFH and host halo assembly history. A number of empirical models relate SFHs of galaxies linearly to their host halo mass accretion rates and successfully reproduce a number of observations (Taghizadeh-Popp et al. 2015; Becker 2015; Rodríguez-Puebla et al. 2016; Mitra et al. 2017; Cohn 2017; Moster et al. 2017). Such models make the strong assumption that SFH of galaxies are perfectly correlated to halo accretion history. Recently by analyzing the observed correlation between the SFRs and large-scale environment of SF galaxies, Tinker et al. (2018a) found the first observational evidence for this correlation, but with a correlation coefficient of  $r \sim 0.63$ . These models, therefore, ignore variation in star formation independent from halo accretion, which may come from physical processes in galaxies. More recently, the empirical model of Behroozi et al. (2019) correlate SFH with halo assembly while also incorporating star formation variability in the SFH. For halos at a given  $v_{M_{\text{peak}}}$  (the maximum circular velocity of the halo at the redshift of max halo mass) and  $z$ , they assign higher SFRs to halos with higher values of  $\Delta v_{\text{max}}$  (logarithmic growth in the maximum circular velocity of the halo over past dynamical time) allowing for random scatter in the assignment. Through this random scatter, which is further separated into contributions from shorter and longer timescales, they incorporate star formation variability. Explicitly examining and constraining the timescale of star formation variability, however, is difficult with such a parameterization. Such constraints can shed light on physical processes involved in galaxy star formation and constrain galaxy feedback models (Sparre et al. 2015). For instance, it can be used to differentiate between physical processes such as galactic feedback interacting with the circumgalactic medium, which would cause longer timescale variations, or internal processes affecting the cold gas in the galaxy, which would cause  $\sim 100$  Myr variations. Using the Feedback In Realistic Environments (FIRE) high resolution cosmological simulations, Hopkins et al. (2014) find that explicit and resolved feedback increases time variability in SFRs. Also using FIRE, Sparre et al. (2017) find that varying the strength of Type II supernova feedback can change the burstiness of SFHs. Governato et al. (2015) find that HI shielding from UV radiation and early feedback from young stars would also produce small scale star formation variability.

In this paper, we construct empirical models to investigate the timescale of star formation variability and the connection between SFH and host halo accretion history of SF central galaxies. Central galaxies constitute the majority of massive galaxies ( $M_* > 10^{9.5} M_\odot$ ) at  $z \sim 0$  (Wetzel et al. 2013)

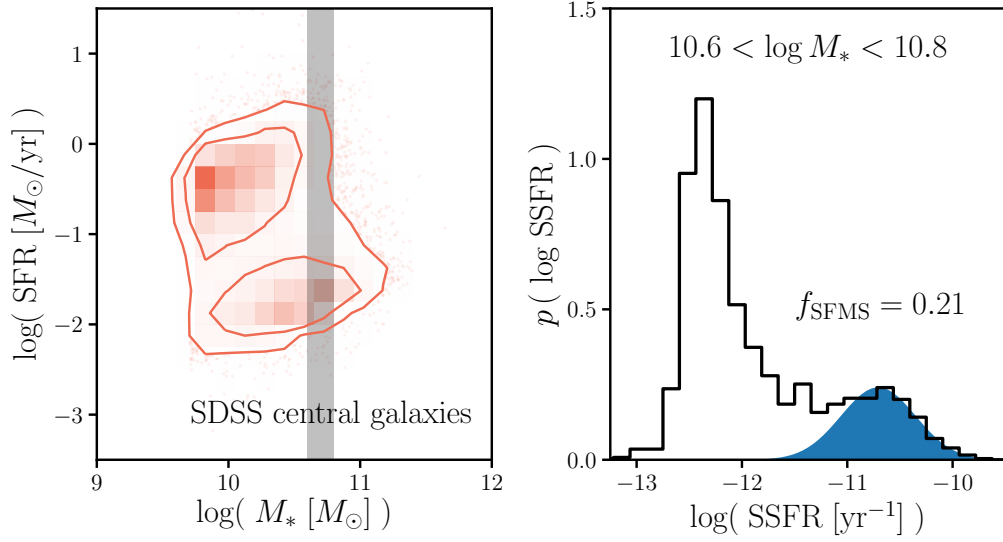


**Figure 1.** The SFR– $M_*$  relation of the central galaxies in SDSS DR7 mark the bimodal distribution of the SF and quiescent populations (left panel). *SF centrals*, based on the correlation between their SFR and  $M_*$ , lie on the so-called “star-forming sequence”. On the right, we present the SSFR distribution,  $p(\log \text{SSFR})$ , of SDSS centrals with  $10.6 < \log M_* < 10.8$ . Based on the SFS component from the Hahn et al. (2018b) GMM fit to the SFR– $M_*$  relation (shaded in blue), galaxies in the SFS account for  $f_{\text{SFS}} = 0.21$  of the centrals in the stellar mass bin.

and their SFHs are not influenced by environmentally-driven external mechanisms that impact SFHs of satellites such as ram pressure stripping (Gunn & Gott 1972; Bekki 2009), strangulation (Larson et al. 1980; Peng et al. 2015), or harassment (Moore et al. 1998). Using a similar approach as Wetzel et al. (2013) and Hahn et al. (2017a), we present models that combine a cosmological  $N$ -body simulation with observed evolutionary trends of the SFS. They statistically track the star formation, stellar mass, and host halo assembly histories of SF central galaxies from  $z \sim 1$  to 0. After fitting our models to reproduce the properties of observed SF central galaxies, we compare the predicted scatter in the SHMR at  $M_h = 10^{12} M_\odot$  (hereafter  $\sigma_{M_*|M_h=10^{12} M_\odot}$ ) of our models to constraints from observations and modern galaxy formation models. This comparison allows us to constrain the timescale of star formation variability and the correlation between SFH and host halo assembly history. Through these comparisons, we examine how our models can produce the constant  $\sigma_{M_*|M_h=10^{12} M_\odot}$  over  $z = 1$  to 0 found in halo model analyses. We also examine how our models can reduce  $\sigma_{M_*|M_h=10^{12} M_\odot}$  from  $z = 1$  to 0 as found in the EAGLE (Matthee et al. 2017) and Illustris TNG (Pillepich et al. 2018) hydrodynamic simulations. Lastly we investigate the impact of varying  $\sigma_{M_*|M_h}(z = 1)$ . In Section 2 we describe the  $z \approx 0$  central galaxy sample used to compare our models that we construct from SDSS Data Release 7. Then in Section 3, we describe the  $N$ -body simulation and how we evolve the SFR and stellar masses of the SF central galaxies in our model. We compare predictions from our model to observations and present the resulting constraints in Section 4. Finally, we conclude and summarize the results in Section 5.

## 2. CENTRAL GALAXIES OF SDSS DR7

We construct our galaxy sample following the sample selection of [Tinker et al. \(2011\)](#). We select a volume-limited sample of galaxies at  $z \approx 0.04$  with  $M_r - 5\log(h) < -18$  and complete above  $M_* > 10^{9.4}h^{-2}M_\odot$  from the NYU Value-Added Galaxy Catalog (VAGC; [Blanton et al. 2005](#)) of the Sloan Digital Sky Survey Data Release 7 (SDSS DR7; [Abazajian et al. 2009](#)). The stellar masses of these galaxies are estimated using the `kcorrect` code ([Blanton & Roweis 2007](#)) assuming a [Chabrier \(2003\)](#) initial mass function. For their specific star formation rates (SSFR) we use measurements from the current release of the MPA-JHU spectral reductions<sup>1</sup> ([Brinchmann et al. 2004](#)). Generally,  $\text{SSFR} > 10^{-11}\text{yr}^{-1}$  are derived from H $\alpha$  emission,  $10^{-11} > \text{SSFR} > 10^{-12}\text{yr}^{-1}$  are derived from a combination of emission lines, and  $\text{SSFR} < 10^{-12}\text{yr}^{-1}$  are based on  $D_n4000$  (see discussion in [Wetzel et al. 2013](#)). We emphasize that  $\text{SSFR} < 10^{-12}\text{yr}^{-1}$  should only be considered upper limits to the actual galaxy SSFR ([Salim et al. 2007](#)).

From this galaxy sample, we identify central galaxies using the [Tinker et al. \(2011\)](#) group finder, a halo-based algorithm that uses the abundance matching ansatz to iteratively assign halo masses to groups (see also [Yang et al. 2005](#)). Every group contains one central galaxy, which by definition is the most massive, and a group can contain zero, one, or many satellites. As with any group finder, galaxies are misassigned due to projection effects and redshift space distortions. Our central galaxy sample has a purity of  $\sim 90\%$  and completeness of  $\sim 95\%$  ([Tinker et al. 2018b](#)). Moreover, as illustrated in [Campbell et al. \(2015\)](#), the [Tinker et al. \(2011\)](#) group finder robustly identifies red and blue centrals as a function of stellar mass, which is highly relevant to our analysis. We present the SFR– $M_*$  relation of the SDSS DR7 central galaxies, described above, in the left panel of [Figure 1](#). The contours of the relation clearly illustrate the bimodality in the galaxy sample with the star-forming centrals lying on the so-call “star-forming sequence” (SFS).

## 3. MODEL: SIMULATED CENTRAL GALAXIES

We are interested in constructing a model that tracks central galaxies and their star formation within the hierarchical growth of their host halos. This requires a cosmological  $N$ -body simulation that accounts for the complex dynamical processes that govern the host halos of galaxies. In this paper we use the high resolution  $N$ -body simulation from [Wetzel et al. \(2013\)](#) generated using the [White \(2002\)](#) `TreePM` code with flat  $\Lambda$ CDM cosmology ( $\Omega_m = 0.274$ ,  $\Omega_b = 0.0457$ ,  $h = 0.7$ ,  $n = 0.95$ , and  $\sigma_8 = 0.8$ ). From initial conditions at  $z = 150$ , generated from second-order Lagrangian Perturbation Theory,  $2048^3$  particles with mass of  $1.98 \times 10^8 M_\odot$  are evolved in a  $250 h^{-1}\text{Mpc}$  ( $357.12 \text{ Mpc}$ ) box with a Plummer equivalent smoothing of  $2.5 h^{-1}\text{kpc}$  ([Wetzel et al. 2013, 2014](#)). ‘Host halos’ are then identified using the Friends-of-Friends algorithm (FoF; [Davis et al. 1985](#)) with linking length of  $b=0.168$  times the mean inter-particle spacing, which links particles with local density  $> \sim 100\times$  the mean matter density. Within these host halos, [Wetzel et al. \(2013\)](#) identifies ‘subhalos’ as overdensities in phase space through a six-dimensional FoF algorithm (FoF6D; [White et al. 2010](#)). The host halos and subhalos are then tracked across the simulation outputs from  $z = 10$  to 0 to build merger

<sup>1</sup> <http://wwwmpa.mpa-garching.mpg.de/SDSS/DR7/>

trees (Wetzel et al. 2009; Wetzel & White 2010). The most massive subhalos in newly-formed host halos at a given simulation output are defined as the ‘central’ subhalo. A central subhalo retains its ‘central’ definition until it falls into a more massive host halo (FoF halo mass), at which point it becomes a ‘satellite’ subhalo.

Throughout its 45 snapshot outs, **TreePM** simulation tracks the evolution of subhalos back to  $z \sim 10$ . We restrict ourselves to 15 snapshots from  $z = 1.08$  to  $0.05$ , where we have the most statistically meaningful observations. Furthermore, since we are interested in centrals we only keep subhalos that are classified as centrals throughout the redshift range. This criterion removes “back splash” or “ejected” satellite galaxies (*e.g.* Mamon et al. 2004; Wetzel et al. 2014) misclassified as centrals. Next, we describe how we select and initialize the SF central galaxies in our model from the central subhalos of the **TreePM** simulation.

### 3.1. Selecting Star-Forming Centrals

To construct a model that tracks the SFR and stellar mass evolution of SF central galaxies, we first need to select them from the central galaxies/subhalos in the **TreePM** simulation. Since we want our model to reproduce observations, our selection is based on  $f_{\text{SFS}}^{\text{cen}}(M_*)$ , the fraction of central galaxies within the SFS measured from the SDSS DR7 VAGC (Section 2). Below, we describe how we derive  $f_{\text{SFS}}^{\text{cen}}(M_*)$  and use it to select SF central galaxies in our model. Afterwards we describe how we initialize the SFRs and  $M_*$  of these galaxies at  $z = 1$ .

Often in the literature, an empirical color-color or SFR– $M_*$  cut that separates the two main modes (red/blue or star-forming/quiescent) in the distribution is chosen to classify galaxies (*e.g.* Baldry et al. 2006; Blanton & Moustakas 2009; Drory et al. 2009; Peng et al. 2010; Moustakas et al. 2013; Hahn et al. 2015). The red/quiescent or blue/star-forming fractions derived from this sort of classification, by construction, depend on the choice of cut and neglect galaxy subpopulations such as transitioning galaxies *i.e.* galaxies in the “green valley”. Instead, for our  $f_{\text{SFS}}^{\text{cen}}(M_*)$ , we use the SFS identified from the Hahn et al. (2018b) method, which uses Gaussian Mixture Models (GMM) and the Bayesian Information Criteria to fit the SFR– $M_*$  relation of a galaxy population and identify its SFS. This data-driven approach relaxes many of the assumptions and hard cuts that go into other methods and can be flexibly applied to a wide range of SFRs and  $M_*$ s and for multiple simulations. The weight of the SFS GMM component from the method provides an estimate of  $f_{\text{SFS}}^{\text{cen}}$ . In the right panel of Figure 1, we present the SSFR distribution,  $p(\log \text{SSFR})$ , of the SDSS DR7 central galaxies within  $10.6 < \log M_* < 10.8$  with the SFS GMM component shaded in blue. The SFS constitutes  $f_{\text{SFS}}^{\text{cen}} = 0.21$  of the SDSS central galaxies in this stellar mass bin. Using the  $f_{\text{SFS}}^{\text{cen}}$  estimates, we fit  $f_{\text{SFS}}^{\text{cen}}$  as a linear function of  $\log M_*$  similar to Wetzel et al. (2013); Hahn et al. (2017a):

$$f_{\text{SFS, bestfit}}^{\text{cen}}(M_*) = -0.627(\log M_* - 10.5) + 0.354. \quad (1)$$

We note that this is in good agreement with the  $f_{\text{Q}}^{\text{cen}}(M_*; z \sim 0)$  fit from Hahn et al. (2017a).

To select the SF centrals from the subhalos, we begin by assigning  $M_*$  at  $z \sim 0$  to the subhalos by abundance matching to  $M_{\text{peak}}$ , the maximum host halo mass that it ever had as a central subhalo (Conroy et al. 2006; Vale & Ostriker 2006; Yang et al. 2009; Wetzel et al. 2012; Leja et al. 2013;

Wetzel et al. 2013, 2014; Hahn et al. 2017a). Abundance matching, in its simplest form, assumes a one-to-one mapping between subhalo  $M_{\text{peak}}$  and galaxy stellar mass,  $M_*$ , that preserves rank order:  $n(>M_{\text{peak}}) > n(>M_*)$ . In practice, we apply a 0.2 dex log-normal scatter in  $M_*$  at fixed  $M_{\text{peak}}$  based on the observed SHMR (e.g. Mandelbaum et al. 2006; More et al. 2011; Velander et al. 2014; Zu & Mandelbaum 2015; Gu et al. 2016; Lange et al. 2018). For  $n(>M_*)$ , we use observed stellar mass function (SMF) from Li & White (2009) at  $z \sim 0$ , which is based on the same SDSS NYU-VAGC sample as our group catalog. Then using the abundance matched  $M_*$ , we randomly select subhalos as SF based on the probabilities of being on the SFS using Eq. 1. Tinker et al. (2017a, 2018b) find that quenching is independent of halo growth rate and therefore we randomly select SF subhalos. In our model, we assume that once a SF galaxy quenches its star formation, it remains quiescent. Without any quiescent galaxies rejuvenating their star formation, galaxies on the SFS at  $z \sim 0$  are also on the SFS at  $z > 0$ . Under this assumption the SF centrals we select at  $z \sim 0$  are also on the SFS at the initial redshift of our model:  $z \sim 1$ .

We next initialize the SF centrals at  $z \sim 1$  using the observed SFR- $M_*$  relation of the SFS with  $M_*$  assigned using abundance matching with a  $z \sim 1$  SMF interpolated between the Li & White (2009) SMF and the SMF from Marchesini et al. (2009) at  $z = 1.6$ . We choose the Marchesini et al. (2009) SMF, among others, because it produces interpolated SMFs that monotonically increase over  $z < 1$ . As noted in Hahn et al. (2017a), at  $z \approx 1$ , the SMF interpolated between the Li & White (2009) and Marchesini et al. (2009) SMFs is consistent with more recent measurements from Muzzin et al. (2013) and Ilbert et al. (2013). We apply a  $\sigma_{M_*|M_h}^{\text{init}} = 0.2$  dex log-normal scatter in the abundance matching based on observations (e.g. Leauthaud et al. 2012; Tinker et al. 2013; Patel et al. 2015). We next assign SFRs based on  $z \sim 1$  observations in the literature. However, observations, not only use galaxy properties derived differently from the SDSS VAGC but they also find SFS with significant discrepancies from one another. In a compilation of SFSs from 25 studies in the literature, Speagle et al. (2014) find that the SFRs of the SFSs at  $z \sim 1$  vary by more than a factor of 2 at  $M_* = 10^{10.5} M_\odot$ , even after their calibration (see Figure 2 of Speagle et al. 2014). With little consensus on the SFS at  $z \sim 1$ , and consequently its redshift evolution, we flexibly parameterize the SFR of the SFS,  $\log \text{SFR}_{\text{SFS}}(M_*, z)$ , with free parameters that characterize the stellar mass dependence of the SFS below and above  $10^{10} M_\odot$  and the redshift dependence ( $m_{M_*}^{\text{low}}$ ,  $m_{M_*}^{\text{high}}$ , and  $m_z$ , respectively):

$$\log \text{SFR}_{\text{SFS}}(M_*, z) = m_{M_*} (\log M_* - 10.) + m_z (z - 0.05) - 0.19 \quad (2)$$

$$\text{where } m_{M_*} = \begin{cases} m_{M_*}^{\text{low}} & \text{for } M_* < 10^{10} M_\odot \\ m_{M_*}^{\text{high}} & \text{for } M_* \geq 10^{10} M_\odot. \end{cases}$$

We assign SFRs to our SF centrals at  $z \sim 1$  by sampling a log-normal distribution centered about  $\log \text{SFR}_{\text{SFS}}(M_*, z=1)$  with a constant scatter of 0.3 dex from observations (Daddi et al. 2007; Noeske et al. 2007; Magdis et al. 2012; Whitaker et al. 2012). Later when comparing to observations, we choose conservative priors for the parameters  $m_{M_*}^{\text{low}}$ ,  $m_{M_*}^{\text{high}}$  and  $m_z$  that encompass the best-fit SFS from Speagle et al. (2014) as well as measurements from Moustakas et al. (2013) and Lee et al. (2015). With our SF centrals initialized at  $z \sim 1$ , next, we describe how we evolve their SFR and  $M_*$ .

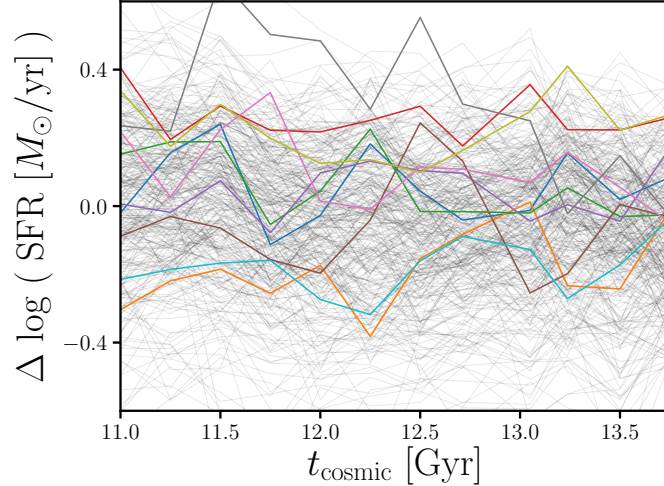


**Figure 2.** SF galaxies in the Illustris hydrodynamical simulation have SFHs that evolve along the SFS, with their SFRs stochastically fluctuating about the mean log SFR of the SFS. We highlight  $\Delta \log \text{SFR}$ , SFR with respect to  $\log \text{SFR}_{\text{SFS}}$  (Eq. 3), for a handful of galaxies with  $10^{10.5} < M_* < 10^{10.6} M_\odot$  at  $z \sim 0$ . We calculate  $\Delta \log \text{SFR}$  with  $\log \text{SFR}_{\text{SFS}}$  identified using the Hahn et al. (2018b) method, same as in Section 3.1. The implementation of SFR variability in the SFHs of SF centrals in our model (Section 3.2) is motivated by the SFHs of Illustris galaxies above.

### 3.2. Evolving along the Star Formation Sequence

The tight correlation between the SFRs and  $M_*$  of SF galaxies on the SFS has been observed spanning over four orders of magnitude in stellar mass, with a roughly constant scatter of  $\sim 0.3$  dex, and out to  $z > 2$  (e.g. Noeske et al. 2007; Daddi et al. 2007; Elbaz et al. 2007; Salim et al. 2007; Santini et al. 2009; Karim et al. 2011; Whitaker et al. 2012; Moustakas et al. 2013; Lee et al. 2015; see also references in Speagle et al. 2014). This correlation is also predicted by modern galaxy formation models (Somerville & Davé 2015, see Hahn et al. 2018b and references therein). The SFS naturally presents itself as an anchoring relationship to characterize the star formation and  $M_*$  growth histories of SF galaxies throughout  $z < 1$ . We, therefore, characterize the SFH of each SF central with respect to the log SFR of the SFS (Eq. 2):

$$\log \text{SFR}_i(M_*, t) = \log \text{SFR}_{\text{SFS}}(M_*, t) + \Delta \log \text{SFR}_i(t). \quad (3)$$

Since SFH determines the  $M_*$  growth of galaxies, in this prescription,  $\Delta \log \text{SFR}_i(t)$  dictates the SFH and  $M_*$  evolution of SF centrals.

One simple prescription for  $\Delta \log \text{SFR}(t)$  would be to keep  $\Delta \log \text{SFR}$  fixed throughout  $z < 1$  to the offsets from the  $\log \text{SFR}_{\text{SFS}}$  in the initial SFRs of our SF centrals at  $z \sim 1$ , similar to simple analytic models such as Mitra et al. (2015). Galaxies with higher than average initial SFRs continue evolving above the average SFS, while SF centrals with lower than average initial SFRs continue evolving below the average SFS. In addition to not being able to reproduce observations, which we later demonstrate, we also do not find such SFHs in SF galaxies of hydrodynamic simulations such as Illustris (Vogelsberger et al. 2014; Genel et al. 2014). In Figure 2, we plot  $\Delta \log \text{SFR}_i$  of SF galaxies in



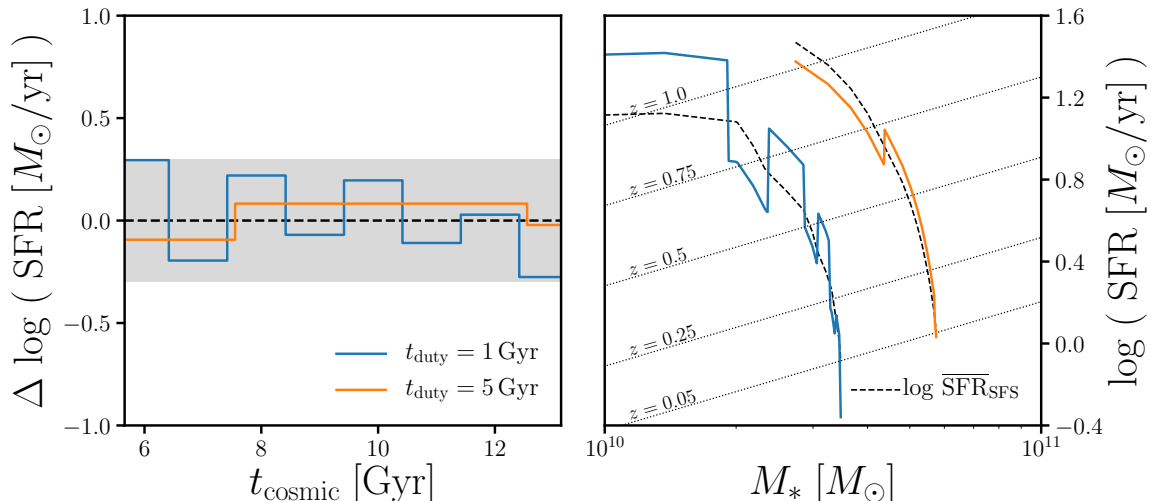


**Figure 3.** We incorporate star formation variability in our model using a “star formation duty cycle” where the SFRs of SF centrals fluctuate about  $\log \text{SFR}_{\text{SFS}}$  on some timescale  $t_{\text{duty}}$ . In our fiducial prescription, we randomly sample  $\Delta \log \text{SFR}_i$  from a log-normal distribution with 0.3 dex scatter at each duty cycle timestep. We illustrate  $\Delta \log \text{SFR}_i(t)$  of two SF centrals with star formation duty cycles on  $t_{\text{duty}} = 1$  (blue) and 5 Gyr (orange) timescales in the left panel.  $\Delta \log \text{SFR}(t)$  determines the SFH and hence the  $M_*$  growth of the SF central galaxies (Eq. 4). On the right, we illustrate the SFR and  $M_*$  evolutions of the corresponding SF centrals. For reference, we include  $\log \text{SFR}_{\text{SFS}}(M_{*,i}(t), t)$  that the galaxies’ SFR and  $M_*$  evolve along (black solid). We also include  $\log \text{SFR}_{\text{SFS}}(M_*)$  at various redshifts between  $z = 1$  to 0.05 (dotted lines). *The SF centrals in our model evolve their SFRs and  $M_*$  along the SFS with their SFRs fluctuate about  $\log \text{SFR}_{\text{SFS}}$ .*

the Illustris simulation as a function of cosmic time. These galaxies have  $10^{10.5} < M_* < 10^{10.6} M_\odot$  at  $z = 0$ . At each simulation output, we calculate  $\Delta \log \text{SFR}_i$  using Eq. 3 with  $\log \text{SFR}_{\text{SFS}}$  derived from the SFS identified in the simulation using the Hahn et al. (2018b) method, same as in Section 3.1. As the highlighted  $\Delta \log \text{SFR}_i$  illustrate, SF galaxies in Illustris evolve along the SFS with their SFRs fluctuating about  $\log \text{SFR}_{\text{SFS}}$ .

Motivated by the SFHs of Illustris SF galaxies, we introduce variability to the SFHs of our SF centrals in the form of a “star formation duty cycle”—*i.e.* we set the SFRs of SF centrals to fluctuate about the SFR of the SFS on some timescale  $t_{\text{duty}}$ . Within the SFH of Eq. 3, we parameterize  $\Delta \log \text{SFR}_i$  to fluctuate about the  $\log \text{SFR}_{\text{SFS}}$  on timescale,  $t_{\text{duty}}$ , with amplitude sampled from a log-normal distribution with 0.3 dex scatter. For our fiducial star formation duty cycle prescription, we randomly sample  $\Delta \log \text{SFR}_i$  from a log-normal distribution with 0.3 dex scatter. We illustrate  $\Delta \log \text{SFR}_i(t)$  of SF centrals with our star formation duty cycle prescription on  $t_{\text{duty}} = 1$  Gyr (blue) and 5 Gyr (orange) timescales in the left panel of Figure 3. The shaded region represents the observed 0.3 dex scatter of  $\log \text{SFR}$  in the SFS. By construction, this  $\Delta \log \text{SFR}$  prescription reproduces the observed log-normal SFR distribution of the SFS at any point in the model. Although, this simplified prescription does not reflect the individual SFHs of SF centrals, we seek to statistically capture the stochasticity from gas accretion, star-bursts, and feedback mechanisms for the entire SF population. Measuring  $t_{\text{duty}}$  in the duty cycle parameterization provides us with an estimate of the timescale

of such star formation variabilities and thus provide a useful constraint on the physics of galaxy formation.

Using our fiducial SFH prescription, we evolve both the SFR and  $M_*$  of our SF centrals along the SFS. Based on Eq. 3, the SFRs of our SF centrals are functions of  $M_*$ , while  $M_*$  is the integral of the SFR over time:

$$M_*(t) = f_{\text{retain}} \int_{t_0}^t \text{SFR}(M_*, t') dt' + M_0. \quad (4)$$

$t_0$  and  $M_0$  are the initial cosmic time and stellar mass at  $z \sim 1$ , respectively.  $f_{\text{retain}}$  here is the fraction of stellar mass that is retained after supernovae and stellar winds; we use  $f_{\text{retain}} = 0.6$  (Wetzel et al. 2013) and assume instantaneous recycling such that  $f_{\text{retain}}$  is applied at all times. We can now evolve the SFR and  $M_*$  of our SF centrals until the final  $z = 0.05$  snapshot by solving the differential equation of Eqs. 3 and 4. On the right panel of Figure 3, we present the SFR and  $M_*$  evolutions of two SF centrals with  $t_{\text{duty}} = 1$  (blue) and 5 Gyr (orange), same as the left panel. For reference, we include the mean  $\log \text{SFR}$  of the SFS that the galaxies' SFR and  $M_*$  evolve along,  $\log \text{SFR}_{\text{SFS}}(M_{*,i}(t), t)$  (black solid). We also include  $\log \text{SFR}_{\text{SFS}}(M_*)$  (dotted lines) at various redshifts between  $z = 1$  to 0.05. Based on the SFH prescription in our model, SF centrals evolve their SFRs and  $M_*$  along the SFS with their SFRs fluctuate about  $\log \text{SFR}_{\text{SFS}}$ .

### 3.3. Correlating SFR with Halo Growth

In our fiducial SFH prescription, we sample  $\Delta \log \text{SFR}_i$  randomly from a log-normal distribution with 0.3 dex scatter. There is, however, growing evidence that star formation in galaxies correlate with their host halo accretion histories (*e.g.* Lim et al. 2016; Tojeiro et al. 2017; Tinker et al. 2018a). In this section, we introduce *assembly bias* into the SFH prescription of our model. Assembly bias, most commonly in the literature, refers to the dependence of the spatial distribution of dark matter halos on halo properties besides mass (Gao et al. 2005; Wechsler et al. 2006; Gao & White 2007; Wetzel et al. 2007; Li et al. 2008; Sunayama et al. 2016). At low halo mass, older and more concentrated halos form in high density environments. While at high halo mass, the effect is the opposite — younger, less concentrated halos form in high-density regions. However, both simulations (Croton et al. 2007; Artale et al. 2018; Zehavi et al. 2018) as well as observations (Yang et al. 2006; Wang et al. 2008; Tinker et al. 2011; Wang et al. 2013; Lacerna et al. 2014; Calderon et al. 2018; Tinker et al. 2018b), find that this assembly bias propagates beyond spatial clustering and correlates with certain galaxy properties such as formation histories and star formation properties, an effect more specifically referred to as *galaxy assembly bias*. In our model, we incorporate galaxy assembly bias by correlating the SFHs of our SF central galaxies and their host halo accretion histories with a correlation coefficient  $r$ .

We correlate  $\Delta \log \text{SFR}$  (Eq. 3) to the halo mass accretion over dynamical time, which we define as  $t_{\text{dyn}} = (\frac{4}{3}\pi G 200\rho_m(t))^{-\frac{1}{2}}$ . At every  $t_{\text{duty}}$  timestep,  $t$ ,  $\Delta \log \text{SFR}(t)$  is assigned based on  $\Delta M_h(t) = M_h(t) - M_h(t - t_{\text{dyn}})$  in  $M_{\text{max}}$  bins with a correlation coefficient  $r$ , an additional parameter to our model. This prescription for correlating  $\Delta \log \text{SFR}$  to  $\Delta M_h$  is similar to other empirical models that also correlate  $\Delta \log \text{SFR}$  to  $\Delta M_h$  over  $t_{\text{dyn}}$  (Rodríguez-Puebla et al. 2016; Behroozi et al. 2019). In

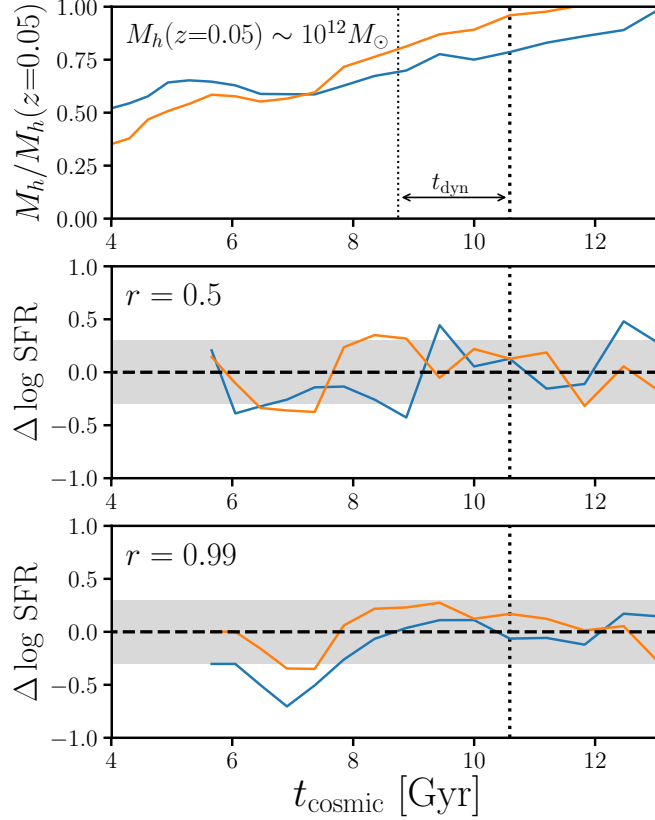


**Figure 4.** We incorporate galaxy assembly bias into the SF centrals of our model by correlating their host halo accretion history to  $\Delta \log \text{SFR}(t)$ , the SFH with respect to the SFS, with correlation coefficient  $r$ . We plot the relative halo accretion history,  $M_h(t)/M_h(z=0.05)$  for two randomly chosen SF centrals with  $M_h(z=0.05) \sim 10^{12} M_\odot$ , in the top panel. In the two panels below, we present  $\Delta \log \text{SFR}$ , of these galaxies for our model with  $r = 0.5$  and  $0.99$  (middle and bottom). The shaded region in these panels mark the  $0.3$  dex  $1\text{-}\sigma$  width of the log-normal SFS. At some  $t$  (dotted),  $\Delta \log \text{SFR}(t)$  is correlated with halo accretion over the period  $t - t_{\text{dyn}}$  to  $t_{\text{dyn}}$  labeled in top panel. The SFHs illustrate how  $\Delta \log \text{SFR}(t)$  correlates with  $\Delta M_h = M_h(t) - M_h(t - t_{\text{dyn}})$  and how  $\Delta \log \text{SFR}(t)$  correlates more strongly with  $\Delta M_h(t)$  with higher  $r$ .

Rodríguez-Puebla et al. (2016), however, they assume perfect ( $r = 1$ ) correlation between SFH and halo accretion. In the Behroozi et al. (2019) UNIVERSEMACHINE (hereafter UM),  $r$  is free parameter and their SFH includes SF variability, similar to our model. As we mention in the introduction, their prescription, however, does not focus on a star formation variation on specific timescales, which our models do through the star formation duty cycle.

In Figure 4, we illustrate our prescription for galaxy assembly bias in our model. We plot the relative halo accretion histories  $M_h(t)/M_h(z=0.05)$  of two arbitrarily chosen SF centrals with  $M_h(z=0.05) \sim 10^{12} M_\odot$  in the top panel (orange and blue). Below, we plot  $\Delta \log \text{SFR}$ , SFH with respect to the SFS, of these galaxies for our model with correlation coefficients  $r = 0.5$  and  $0.99$  (middle and bottom). We choose a random TreePM snapshot,  $t$  (dotted), and label the period  $[t, t - t_{\text{dyn}}]$ . Halo accretion over this period,  $\Delta M_h = M_h(t) - M_h(t - t_{\text{dyn}})$ , correlates with  $\Delta \log \text{SFR}(t)$ .

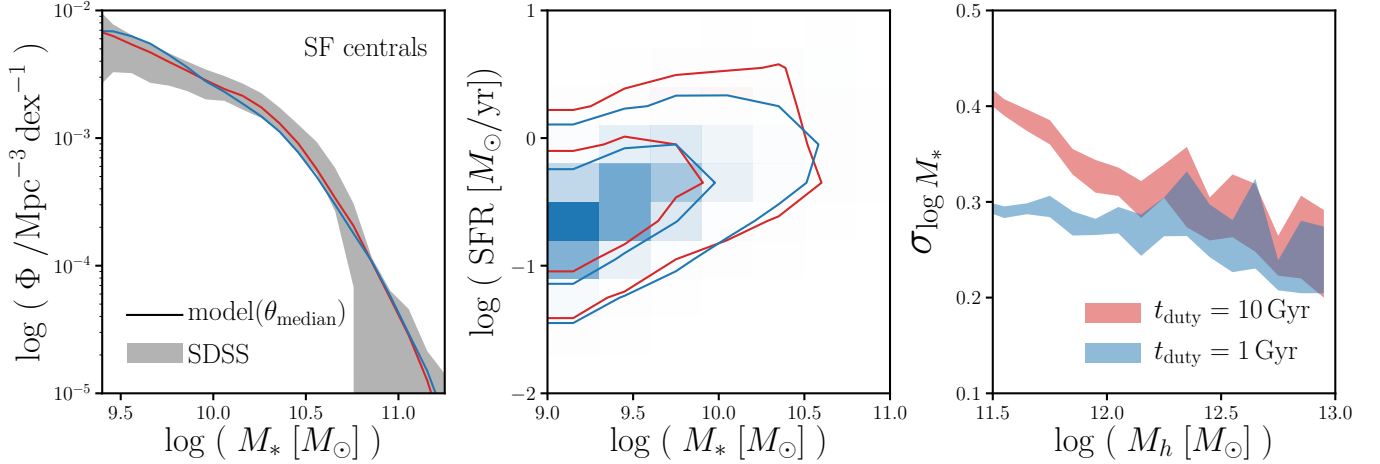


**Figure 5.** Our models with different star formation duty cycle timescales ( $t_{\text{duty}} = 1$  and 5 Gyr; blue and red) run with median values of their ABC posterior distribution produce SMFs and SFs consistent with observations (left and middle). They however predict significantly different scatter in  $\log M_*$  at fixed  $\log M_{\text{halo}}$  for SF centrals —  $\sigma_{M_*|M_h}$  (right). By comparing the scatter in SHMR of our models to observational constraints on the SHMR, we can constrain the timescale of the star formation duty cycle and thereby the SFHs of star forming galaxies.

The SFHs in the middle and bottom panels illustrate this correlation and how  $\Delta \log \text{SFR}(t)$  correlates more strongly with  $\Delta M_h(t)$  for our model with higher  $r$ .

### 3.4. SHMR scatter at $z = 1$

So far in both our fiducial and galaxy assembly bias added models above, we assume that the log-normal scatter in  $M_*$  at fixed  $M_h$  at  $z \sim 1$ :  $\sigma_{M_*|M_h}^{\text{init}} = 0.2$  dex. This initial condition determines the initial abundance matching  $M_*$  at  $z \sim 1$  that initializes our models and is motivated by constraints on the observed SHMR (*e.g.* Leauthaud et al. 2012; Tinker et al. 2013; Patel et al. 2015). However, these constraints are derived using halo models in which the scatter is a constant, independent of  $M_h$ . For these models, the constraining power mainly come from massive halos. Hence, 0.2 dex does not accurately reflect the SHMR scatter at  $z \sim 1$  for less massive halos ( $M_h \lesssim 10^{12} M_\odot$ ). Later in this paper, we focus on  $\sigma_{M_*|M_h=10^{12} M_\odot}(z=0)$  predicted by our models. We therefore examine the impact of varying  $\sigma_{M_*|M_h}^{\text{init}}$  on  $\sigma_{M_*|M_h=10^{12} M_\odot}$  using models with  $\sigma_{M_*|M_h}^{\text{init}} = 0.35$  and 0.45 dex. Our choice of  $\sigma_{M_*|M_h}^{\text{init}}$  is based on the  $z = 1$  SHMR in the Illustris TNG which has  $\sigma_{\log M_*}(z \sim 1)$  spanning 0.45 to 0.3 dex for  $M_h = 10^{11.5}$  to  $10^{12} M_\odot$ .

All of the models we present in this section track the SFRs and  $M_*$  of SF central galaxies. We can compare these properties of our model galaxies to observed galaxy population statistics (quiescent fraction and SMF) to constrain the free parameters. Our models, run with these inferred parameters, can then be compared to observations of the galaxy-halo connection such as the SHMR. In the following section, we present this comparison and the constraints we derive on the role and timescale of star formation variability in SF central galaxies.

## 4. RESULTS AND DISCUSSION

Our models take `TreePM` central subhalos and tracks their SFR and  $M_*$  evolution using flexible parameterizations of the SFS and SFHs that incorporate variability through a star formation duty cycle. At  $z = 0.05$ , the final timestep, our models predict SFR and  $M_*$  of SF centrals, along with their host halo properties. We now use these predicted properties to compare our model to observations and constrain its free parameters — the SFS parameters of Eq. 2. Since we focus on SF centrals, for our observations we use the SMF of SF centrals in SDSS, which we estimate as

$$\Phi_{\text{SF, cen}}^{\text{SDSS}} = f_{\text{SFS}}^{\text{cen}} \times f_{\text{cen}} \times \Phi^{\text{Li\&White(2009)}}. \quad (5)$$

$f_{\text{SFS}}^{\text{cen}}$  is the fraction of central galaxies on the SFS, which we fit in Eq. 1.  $f_{\text{cen}}$  is the central galaxy fraction from [Wetzel et al. \(2013\)](#) and  $\Phi^{\text{Li\&White(2009)}}$  is the SMF of the SDSS from [Li & White \(2009\)](#). If our models reproduce the observed  $\Phi_{\text{SF, cen}}^{\text{SDSS}}$ , by construction they reproduce the observed quiescent fraction.

For the comparison between our models and observation, we use the likelihood-free parameter inference framework of Approximate Bayesian Computation (ABC). ABC has the advantage over standard approaches to parameter inference in that it does not require evaluating the likelihood. For observables with likelihoods that are difficult or intractable, incorrect assumptions in the likelihood can significantly bias the posterior distributions (*e.g.* [Hahn et al. 2018a](#)). Instead, ABC relies only on a simulation of the observed data and a distance metric to quantify the “closeness” between the observed data and simulation. Many variations of ABC has been used in astronomy and cosmology (*e.g.* [Cameron & Pettitt 2012](#); [Weyant et al. 2013](#); [Ishida et al. 2015](#); [Alsing et al. 2018](#)). We use ABC in conjunction with the efficient Population Monte Carlo (PMC) importance sampling as in [Hahn et al. \(2017a,b\)](#). For initial sampling of our ABC particles, *i.e.* the priors of our free parameters  $m_{M_*}^{\text{low}}$ ,  $m_{M_*}^{\text{high}}$ , and  $m_z$ , we use uniform distributions over the ranges [0.0, 0.8], [0.0, 0.8], and [0.5, 2.0], respectively. The range of the prior were conservatively chosen to encompass the best-fit SFS from [Speagle et al. \(2014\)](#) as well as measurements from [Moustakas et al. \(2013\)](#) and [Lee et al. \(2015\)](#) at  $z \sim 1$ . Finally, for our distance metric we use the following distance between the SMF of the star-forming centrals in our model to the observed  $\Phi_{\text{SF, cen}}^{\text{SDSS}}$ :

$$\rho_{\Phi} = \sum_M \left( \frac{\Phi^{\text{sim}} - \Phi_{\text{SF, cen}}^{\text{SDSS}}}{\sigma'_{\Phi}} \right)^2. \quad (6)$$

$\Phi^{\text{sim}}(M)$  above is the SMF of the SF centrals in our model and  $\sigma'_{\Phi}(M)$  is the uncertainty of  $\Phi_{\text{SF, cen}}^{\text{SDSS}}$ , which we derive by scaling the [Li & White \(2009\)](#) uncertainty of  $\Phi^{\text{SDSS}}$  derived from mock catalogs. For the rest of our ABC-PMC implementation, we strictly follow the implementation of [Hahn et al. \(2017b\)](#) and [Hahn et al. \(2017a\)](#). We refer reader to those papers for further details.

#### 4.1. The Fiducial Model

We present the SMFs (left), SFSs (center), and  $\sigma_{M_*|M_h}(M_h)$  (right) of our fiducial model run using SFHs with  $t_{\text{duty}}=10$  (red) and 1 Gyr (blue) duty cycle timescales in Figure 5. For each  $t_{\text{duty}}$ , we evaluate our fiducial model using the median of the posterior parameter distributions derived from ABC. For both  $t_{\text{duty}}$ , our model successfully produces SMFs,  $\Phi_{\text{SF, cen}}^{\text{SDSS}}$ , and SFSs consistent with

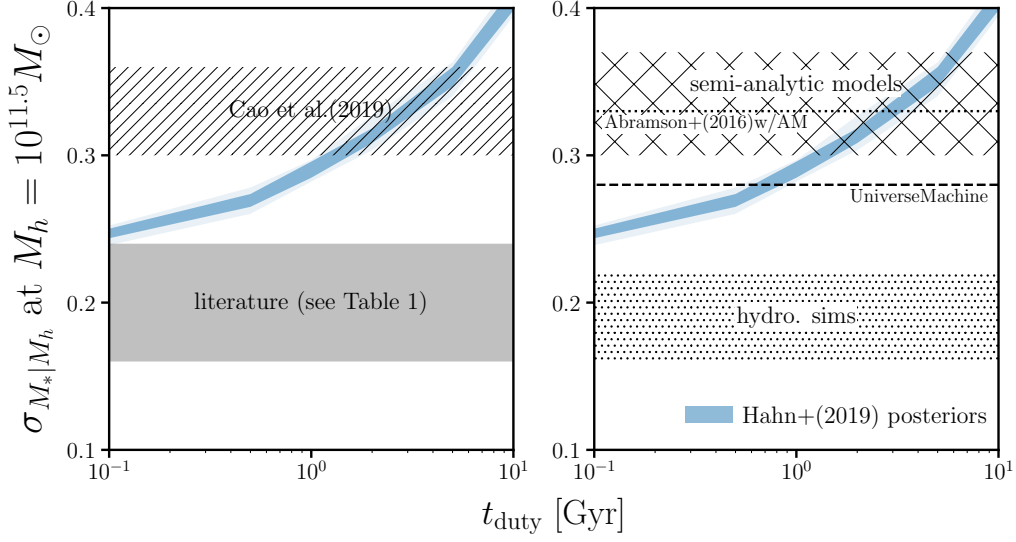


**Figure 6.** With shorter star formation duty cycle timescales,  $t_{\text{duty}}$ , our fiducial model predicts smaller scatter in  $\log M_*$  at  $M_h = 10^{12} M_\odot$  —  $\sigma_{M_*|M_h=10^{12} M_\odot}$  (blue). The dark and light blue shaded regions represent the 68% and 95% confidence intervals of the predicted scatter from the ABC posteriors of our model with  $t_{\text{duty}} = 0.1 - 10$  Gyr. For  $t_{\text{duty}} = 10$  to 0.1 Gyr,  $\sigma_{M_*|M_h=10^{12} M_\odot}$  ranges from  $0.32^{+0.02}_{-0.02}$  to  $0.26^{+0.01}_{-0.01}$ . In the left panel, we include for comparison observational  $\sigma_{M_*|M_h}$  constraints from Leauthaud et al. (2012); Zu & Mandelbaum (2015); Tinker et al. (2017b); Lange et al. (2018) within the shaded region and Cao et al. (in preparation) in the diagonally hatched region (see Section 4.1 and 1). In the right panel, we include compiled predictions from hydrodynamic simulations (dotted region; EAGLE, Massive Black II, Illustris TNG), semi-analytic models (hatched), and the Behroozi et al. (2019) UM empirical model. We also include  $\sigma_{M_*|M_h=10^{12.4} M_\odot}$  from a simple empirical model with Abramson et al. (2016) SFHs assigned to halos via abundance matching (dotted). A shorter  $t_{\text{duty}}$  produces significantly tighter scatter in the SHMR. Halo model observations constraints and predictions from hydrodynamic simulations favor a star formation variability on  $t_{\text{duty}} \lesssim 0.1$  Gyr for our fiducial model.

observations (left and center panels). Despite reproducing observations, the fiducial model with different  $t_{\text{duty}}$  predict significantly different  $\sigma_{M_*|M_h}$ , particularly below  $M_h < 10^{12.5} M_\odot$ . We further illustrate the sensitivity of  $\sigma_{M_*|M_h}$  predicted by our model to  $t_{\text{duty}}$  in Figure 6, where we present  $\sigma_{M_*|M_h}$  at fixed  $M_h = 10^{12} M_\odot$  for our model with  $t_{\text{duty}} = 0.1 - 10$  Gyr.  $\sigma_{M_*|M_h}$  at  $t_{\text{duty}}$  is the prediction from our model run using parameters from the corresponding ABC posterior distributions. The dark and light blue shaded regions represents the 68% and 95% confidence intervals. For  $t_{\text{duty}} = 10$  to 0.1 Gyr,  $\sigma_{M_*|M_h=10^{12} M_\odot}$  ranges from  $0.32^{+0.02}_{-0.02}$  to  $0.26^{+0.01}_{-0.01}$  — a shorter star formation duty cycle timescale produces significantly tighter scatter in the SHMR. This difference is even larger for  $\sigma_{M_*|M_h}$  at  $M_h = 10^{11.5} M_\odot$ : for  $t_{\text{duty}} = 10$  to 0.1 Gyr,  $\sigma_{M_*|M_h=10^{11.5} M_\odot} = 0.41^{+0.01}_{-0.01}$  to  $0.25^{+0.004}_{-0.003}$ . We focus on  $\sigma_{M_*|M_h=10^{12} M_\odot}$  where there are more robust constraints from observations and galaxy formation models. Hence, *the scatter in the SHMR, particular  $\sigma_{M_*|M_h < 10^{12} M_\odot}$ , can be used to probe the star variability timescale and SFH of SF central galaxies.*

**Table 1.**  $\sigma_{M_*|M_h}$  constraints in the literature

	observations	method	$\sigma_{M_* M_h}$
Leauthaud et al. (2012)	COSMOS: SMF, galaxy clustering, galaxy-galaxy lensing	HOD	$0.206^{+0.031}_{-0.021}$
Reddick et al. (2013)	SDSS DR7: satellite kinematics, projected galaxy clustering, conditional SMF	abundance matching	$0.21^{+0.025}_{-0.025}$
Zu & Mandelbaum (2015)	SDSS DR7: galaxy clustering, galaxy-galaxy lensing	HOD	$0.22^{+0.02}_{-0.02}$
Tinker et al. (2017b)	BOSS: projected galaxy clustering	abundance matching	$0.18^{+0.01}_{-0.02}$
Lange et al. (2018)*	SDSS DR7: conditional luminosity function, radial profile of satellite galaxies	HOD	$0.23^{+0.018}_{-0.018}$
Cao et al. in prep.	SDSS DR7: kurtosis of line-of-sight pairwise velocity distribution		$0.33^{+0.03}_{-0.03}$

\*Lange et al. (2018) constrain  $\sigma_{L|M_h}$  instead of  $\sigma_{M_*|M_h}$ .

On the left panel of Figure 6, we compare  $\sigma_{M_*|M_h=10^{12}M_\odot}$  predictions from our fiducial model to observational constraints in the literature. These constraints are mainly derived from fitting halo-occupation based models to observations of galaxy clustering, SMF, satellite kinematics, or galaxy-galaxy weak lensing. We include constraints from Leauthaud et al. (2012); Reddick et al. (2013); Zu & Mandelbaum (2015); Tinker et al. (2017b), and Lange et al. (2018) in the shaded region as well as Cao et al. (in preparation) in the diagonally hatched region. The width of the shaded and hatched regions encompass the 1- $\sigma$  uncertainties of the constraints. Reddick et al. (2013), and Zu & Mandelbaum (2015) fit SDSS DR7 measurements of satellite kinematics, projected galaxy clustering and conditional SMF, and galaxy clustering and galaxy-galaxy lensing, respectively. Tinker et al. (2017b) similarly fit the projected galaxy clustering of the Baryon Oscillation Spectroscopic Survey (Dawson et al. 2013). Meanwhile, Leauthaud et al. (2012) use COSMOS to fit the SMF, galaxy clustering, and galaxy-galaxy lensing. Finally, Cao et al. (in preparation) fit the kurtosis of the line-of-sight pairwise velocity dispersion between central galaxies and all neighboring galaxies to constrain the scatter in SHMR at low halo masses. We note that Leauthaud et al. (2012); Reddick et al. (2013); Zu & Mandelbaum (2015); Tinker et al. (2017b) measure  $\sigma_{M_*|M_h}$  for all central galaxies, not only SF. However, Tinker et al. (2013) find little ( $< 1\sigma$ ) difference in  $\sigma_{M_*|M_h}$  between SF and quiescent centrals, so we include these constraints in our comparison. We also include the Lange et al. (2018) constraint from fitting color-dependent conditional luminosity function and radial profile of satellite galaxies of SDSS DR7. This constraint, however, is on the scatter in luminosity,  $\log L$ , not  $\log M_*$  at a given  $M_h$ . We list the constraints from the literature in Table 1.

Overall, observational constraints are more consistent with  $\sigma_{M_*|M_h}$  predictions of our fiducial model with a short,  $< 1$  Gyr, duty cycle timescale. However, there is no clear consensus among the observed  $\sigma_{M_*|M_h}$  constraints. Besides Cao et al. (in preparation), the  $\sigma_{M_*|M_h}$  constraints in the literature are loosely consistent with  $\sim 0.2$  dex. These constraints, however, are mostly derived using halo models that assume  $\sigma_{M_*|M_h}$  is a constant, independent of  $M_h$ . The constraining power for these constraints mainly come from high mass halos and, thus, do not reflect  $\sigma_{M_*|M_h}$  at  $M_h = 10^{12} M_\odot$ . While Reddick et al. (2013) constrain  $\sigma_{M_*|M_h}$  for different bins of  $M_h$  over the range  $10^{12} - 10^{14} M_\odot$ , their constraints mainly come from halos with  $M_h \geq 10^{13} M_\odot$  (Wechsler & Tinker 2018). The constraint from Lange et al. (2018) is also derived from a halo model with  $M_h$  dependence. However, as mentioned above, they constrain  $\sigma_{L|M_h}$ . In More et al. (2011), where they constrain both  $\sigma_{L|M_h}$  and  $\sigma_{M_*|M_h}$  from the same sample, they find  $\sigma_{M_*|M_h} = 0.15^{+0.08}_{-0.11} < \sigma_{L|M_h} = 0.21^{+0.06}_{-0.04}$  for blue centrals. Translating  $\sigma_{L|M_h}$  to  $\sigma_{M_*|M_h}$ , however, is tenuous for different data sets and models. We also note observational constraints include significant measurement uncertainties in  $M_*$ . The intrinsic  $\sigma_{M_*|M_h}$  of these constraints, *i.e.* the scatter predicted by our model, will be lower. If we consider  $0.1 - 0.2$  dex uncertainties in  $M_*$  (Roediger & Courteau 2015), the Cao et al. (in preparation) constraint, for instance, will be reduced from  $\sigma_{M_*|M_h} = 0.33$  dex to  $0.31 - 0.26$  dex.

In addition to the observational constraints, we also compare the  $\sigma_{M_*|M_h=10^{12} M_\odot}$  predicted by our model to predictions from modern galaxy formation models on the right panel: hydrodynamic simulations (dot filled), semi-analytic models (SAM; cross hatched), and an empirical model (dashed line). For the large-volume hydrodynamic simulations, the dotted region,  $\sigma_{M_*|M_h=10^{12} M_\odot} = 0.16 - 0.22$  dex, encompasses predictions from EAGLE (Matthee et al. 2017), Massive Black II (Khandai et al. 2015), and Illustris TNG, as compiled in Figure 8 of Wechsler & Tinker (2018). For the SAMs, the cross hatched region,  $\sigma_{M_*|M_h=10^{12} M_\odot} = 0.3 - 0.37$  dex, includes predictions from Lu et al. (2014); Somerville et al. (2012) and the SAGE<sup>2</sup> model (Croton et al. 2016). We also include the prediction from the Behroozi et al. (2019) UM empirical model. Similar to observations, there is little consensus among the  $\sigma_{M_*|M_h}$  predictions of the galaxy formation models.  $\sigma_{M_*|M_h}$  from SAMs are consistent with our model with  $t_{\text{duty}} \gtrsim 5$  Gyr. UM, which predicts a lower  $\sigma_{M_*|M_h}$ , is consistent with  $t_{\text{duty}} = 1 - 5$  Gyr. Lastly, large-volume hydrodynamic simulations predict the lowest  $\sigma_{M_*|M_h}$  among the models with  $\sim 0.2$  dex, which our fiducial model struggles to reproduce even with  $t_{\text{duty}} = 0.1$  Gyr. We note that while there is yet no consensus among the observational  $\sigma_{M_*|M_h}$  constraints at  $M_h = 10^{12} M_\odot$ , at higher  $M_h$  observations are in better agreement and *only* hydrodynamic simulations predict  $\sigma_{M_*|M_h}$  consistent with these observations (Wechsler & Tinker 2018). Right below  $M_h = 10^{12} M_\odot$ , however, hydrodynamic simulations predict significantly higher scatter —  $\sigma_{M_*|M_h}(M_h \sim 10^{11.5}) = 0.22 - 0.32$  dex (Wechsler & Tinker 2018).

Given the little consensus among the actual  $\sigma_{M_*|M_h}$  constraints at  $z = 0$  from both observations and simulations, we examine the redshift evolution trend of  $\sigma_{M_*|M_h}$  from  $z = 1$  to  $0$ . For our model  $\sigma_{M_*|M_h}$  at  $z = 1$  is an input initial condition we use to determine the initial abundance matching  $M_*$  of our model that we set to  $0.2$  dex, based on halo model observations (*e.g.* Leauthaud et al.

<sup>2</sup> <https://tao.asvo.org.au/tao/>



2012; Tinker et al. 2013; Patel et al. 2015). According to our predictions,  $\sigma_{M_*|M_h=10^{12}M_\odot}$  increases by 0.06 – 0.12 dex for  $t_{\text{duty}} = 0.1 - 10$  Gyr. In comparison, halo model observational constraints find constant  $\sigma_{M_*|M_h} = 0.2$  dex evolution. Meanwhile in Illustris TNG,  $\sigma_{M_*|M_h=10^{12}M_\odot}$  decreases over the redshift range from  $\sim 0.3$  dex at  $z = 1$  to  $\sim 0.2$  dex at  $z = 0$  (Cao et al. in preparation). Both of these  $\sigma_{M_*|M_h}$  evolution trends, despite their difference, favor a short duty cycle. However, even with the shortest duty cycle, we find an increasing  $\sigma_{M_*|M_h=10^{12}M_\odot}$  from  $z = 1$ .

#### 4.2. Log-Normal SFH

A key element of our models is the SFH prescription for SF central galaxies where the SFH evolves about the SFS. Contrary to our SFH prescription, Kelson (2014), for example, argue that the SFS is a consequence of central limit theorem and can be reproduced even if *in situ* stellar mass growth is modeled as a stochastic process like a random walk. Gladders et al. (2013); Abramson et al. (2015, 2016), similarly argue that  $\sim 2000$  loosely constrained log-normal SFHs can reproduce observations such as the SMF at  $z \leq 8$  and the SFS at  $z \leq 6$ . These works, however, focus on reproducing observations of galaxy properties and do not examine the galaxy-halo connection such as the SHMR. In order to test whether log-normal SFHs can also produce realistic SHMRs, we construct a simple empirical model using the SFHs,  $\text{SFR}(t)$  and  $M_*(t)$ , from Abramson et al. (2016) and assign them to halos by abundance matching their  $M_*$  to  $M_h$  at  $z \sim 1$ . We then restrict the SFHs to those that would be classified as SF based on a log SSFR  $> -11$  cut. Afterwards we measure  $\sigma_{M_*|M_h}$  at the lowest  $M_h$  where it can be reliably measured given the Abramson et al. (2016) sample's  $M_* > 10^{10}M_\odot$  limit. We find that the Abramson et al. (2016) based empirical model predicts a scatter of  $\sigma_{M_*|M_h}(M_h = 10^{12.4}M_\odot) = 0.33 \pm 0.04$  (dotted; right panel of Figure 6). Although the Abramson et al. (2016) SFHs can reproduce various galaxy properties, the empirical model we construct with them struggles to produce  $\sigma_{M_*|M_h}$  comparable to observational constraints and predictions from UM and hydrodynamic simulations. It also struggles to keep  $\sigma_{M_*|M_h}$  evolution constant or decreasing with redshift. The Abramson et al. (2016) based empirical model that we explore utilizes a simple abundance matching scheme. Diemer et al. (2017) find that their their log-normal fits to the SFHs of Illustris galaxies correlate with halo formation histories. Incorporating such correlations into the abundance matching may reduce  $\sigma_{M_*|M_h}$ .

In this section we demonstrate that star formation variability in the SFH impacts  $\sigma_{M_*|M_h=10^{12}M_\odot}$ : star formation variability on shorter timescales significantly reduces  $\sigma_{M_*|M_h=10^{12}M_\odot}$ . Given this dependence,  $\sigma_{M_*|M_h}$  can conversely be used to constrain the timescale of star formation variability. Although there is no clear consensus in the  $\sigma_{M_*|M_h=10^{12}M_\odot}$  of observations or simulations, overall they favor our model with short variability timescales  $\sim 0.1$  Gyr. However, we find that star formation variability alone is insufficient in producing the tight SHMR scatter and  $\sigma_{M_*|M_h}$  redshift evolution trend found in halo model observations and hydrodynamic simulations. In the next section, we explore how correlation between SFH and halo formation histories impacts  $\sigma_{M_*|M_h=10^{12}M_\odot}$  using our models with galaxy assembly bias.

#### 4.3. Models with Galaxy Assembly Bias: $r > 0$

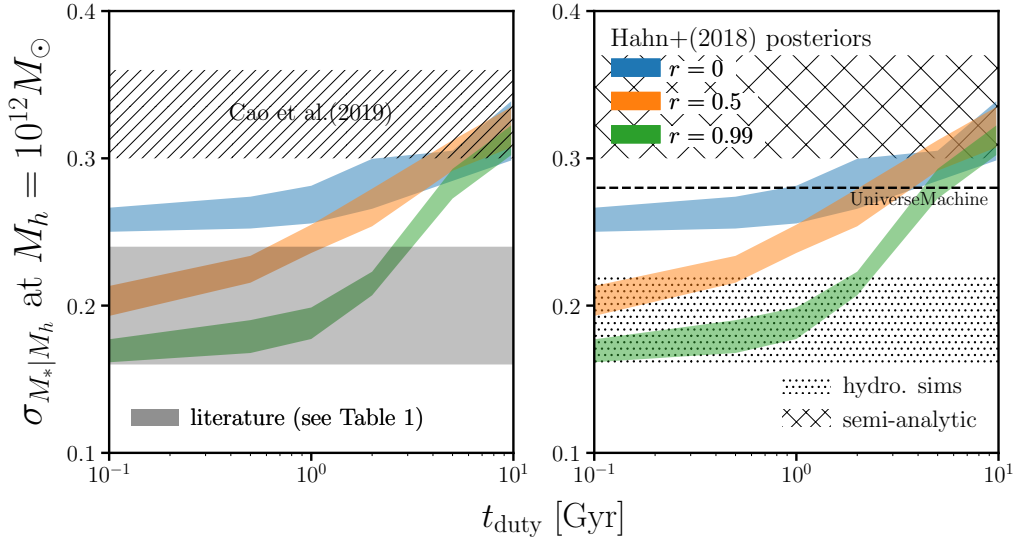


**Figure 7.** Using models that correlate SFH with halo assembly history, we find that higher  $r$ , *i.e.* stronger galaxy assembly bias, significantly reduces the scatter in SHMR for  $t_{\text{duty}} < 5$  Gyr. We plot  $\sigma_{M_*|M_h=10^{12}M_\odot}$  as a function of the star formation duty cycle timescale,  $t_{\text{duty}}$ , for our models with  $r = 0$  (no assembly bias; blue), 0.5 (orange), and 0.99 (green). We include observational constraints and predictions from galaxy formation models in the left and right panels, respectively. With  $r > 0.5$ , our models can predict  $\sigma_{M_*|M_h=10^{12}M_\odot}$  more consistent with the tight  $\sim 0.2$  dex constraint from halo model observations and hydrodynamic simulations.  $r > 0$  also reduces the growth in  $\sigma_{M_*|M_h=10^{12}M_\odot}$  evolution from  $z = 1$  to 0.

A shorter star formation duty cycle timescale produces tighter scatter in the SHMR of our fiducial model. This dependence on the duty cycle timescale, allows us to compare the model to measurements of  $\sigma_{M_*|M_h=10^{12}M_\odot}$  and predictions from galaxy formation models to constrain  $t_{\text{duty}}$ , which reflect the star formation variability timescale. Such comparisons in the previous section, demonstrate that  $t_{\text{duty}} \lesssim 0.5$  Gyr is favored by observational constraints. However, a short duty cycle timescale alone is not enough to reproduce  $\sigma_{M_*|M_h}$  constraints and its evolutionary trend from halo model observations and hydrodynamic simulations. In this section, we examine how assembly bias impacts  $\sigma_{M_*|M_h}$  using our models that correlate SFH with host halo accretion history ( $r > 0$ ).

We repeat our analysis of inferring model parameters by comparing to observations using ABC-PMC — this time for our model with galaxy assembly bias over a grid of  $t_{\text{duty}}$  and  $r$  values. Using the resulting posterior distributions, we examine  $\sigma_{M_*|M_h=10^{12}M_\odot}$  predicted by our model as a function of  $t_{\text{duty}}$  with  $r = 0$  (no assembly bias; blue), 0.5 (orange), and 0.99 (green) in Figure 7. The shaded regions represent the 68% confidence interval of the predicted  $\sigma_{M_*|M_h=10^{12}M_\odot}$ . We again emphasize that for all sets of  $(t_{\text{duty}}, r)$  our models reproduce the observed SMF of SF centrals and SFS. At  $t_{\text{duty}} \geq 5$  Gyr we find no significant difference in the scatter, regardless of  $r$ . Below  $t_{\text{duty}} < 5$  Gyr, however,  $\sigma_{M_*|M_h=10^{12}M_\odot}$  of our model decreases significantly as the SFH of SF galaxies are more correlated with halo accretion history. For  $t_{\text{duty}} = 0.1$  Gyr, we find  $\sigma_{M_*|M_h=10^{12}M_\odot} = 0.26^{+0.01}_{-0.01}$ ,  $0.21^{+0.01}_{-0.01}$ , and  $0.17^{+0.01}_{-0.01}$  for  $r = 0.0, 0.5$ , and  $0.99$ , respectively.

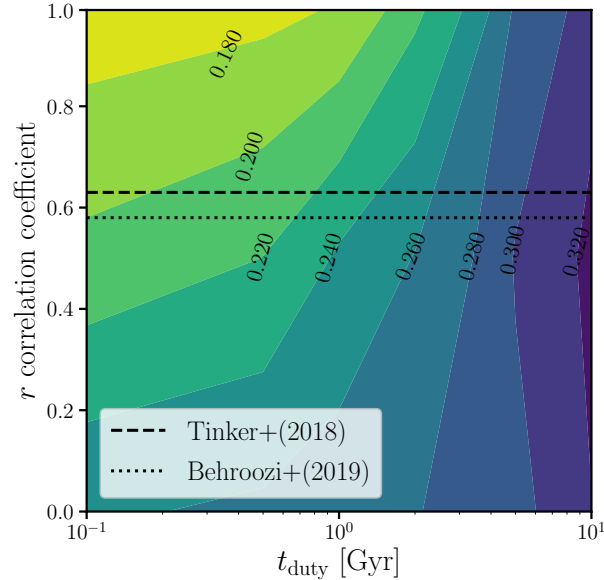


**Figure 8.** Predicted  $\sigma_{M_*|M_h}$  as a function of  $t_{\text{duty}}$  and  $r$  for our models illustrate the degeneracy between the timescale of SF variability and the correlation between SFH and halo assembly history. Based on  $r$  constraints from Tinker et al. (2018a) (dashed) and Behroozi et al. (2019) (dotted),  $t_{\text{duty}} < 0.5$  Gyr is necessary to produce  $\sigma_{M_*|M_h} \sim 0.2$  dex from observations and hydrodynamic simulations. Meanwhile,  $t_{\text{duty}} < 5$  Gyr is necessary to produce  $\sigma_{M_*|M_h}$  from Cao et al. (in preparation), SAMs, and UM.

Comparing our  $r > 0$  models to the observational constraints, we find that galaxy assembly bias significantly reduces the tensions with halo model observations (left panel of Figure 7). With a short star formation duty cycle ( $t_{\text{duty}} \leq 1$  Gyr) and galaxy assembly bias with  $r \geq 0.5$ , our model is in agreement with these  $\sigma_{M_*|M_h} \sim 0.2$  dex constraints. On the other hand, assembly bias increases the tension with Cao et al. (in preparation), which more specifically constrains  $\sigma_{M_*|M_h}$  at  $M_h \sim 10^{12} M_\odot$ . We also compare our  $r > 0$  models to predictions from galaxy formation models on the right panel. By varying  $r$  and  $t_{\text{duty}}$ , our model can reproduce the widely varying galaxy formation model  $\sigma_{M_*|M_h=10^{12} M_\odot}$  predictions. Focusing on hydrodynamic simulations, which best reproduce  $\sigma_{M_*|M_h}$  observations at high  $M_h$ , we find that with a short duty cycle timescale,  $t_{\text{duty}} < 1$  Gyr, and  $r > 0.5$  our models produces the predicted  $\sim 0.2$  dex scatter in SHMR.

A shorter  $t_{\text{duty}}$  or higher  $r$  both produce smaller  $\sigma_{M_*|M_h=10^{12} M_\odot}$ . We highlight this degeneracy in Figure 8, where we plot  $\sigma_{M_*|M_h=10^{12} M_\odot}$  (contour and color map) as a function of  $t_{\text{duty}}$  and  $r$ . Figure 8 more precisely reveals that to produce  $\sigma_{M_*|M_h} \sim 0.2$  dex,  $t_{\text{duty}} \leq 1.5$  Gyr and  $r > 0.7$  (top left corner of Figure 8). In the literature, Tinker et al. (2018a) find correlation between  $\dot{M}_h$  and  $\log \text{SSFR}$  with  $r = 0.63$  (dashed) and Behroozi et al. (2019) similarly find a correlation between SFH and halo assembly history with  $r_c \sim 0.6$  for halos with  $M_h \sim 10^{12} M_\odot$  (dotted). For galaxy assembly bias with  $r = 0.6$ , the shortest timescale we probe ( $t_{\text{duty}} = 0.1$  Gyr) is necessary to produce  $\sigma_{M_*|M_h=10^{12} M_\odot} \sim 0.2$  dex as found in halo model observations and hydrodynamic simulations. This timescale is shorter than the  $\sim 0.5$  Gyr timescale that Sparre et al. (2015) find in Illustris galaxies using a Principal

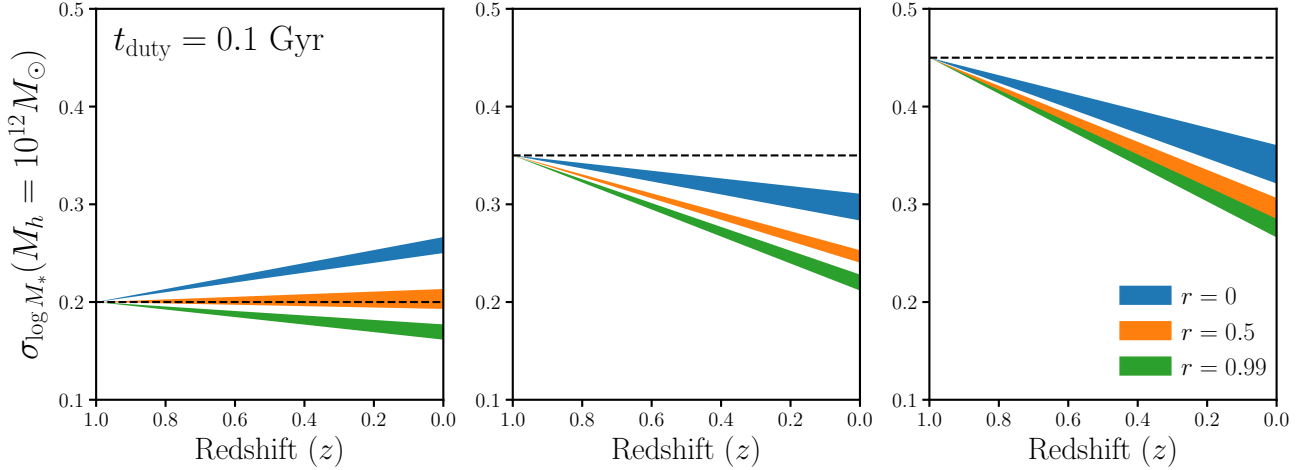


**Figure 9.** The evolution of  $\sigma_{M_*|M_h=10^{12}M_\odot}$  from  $z = 1$  to 0 for our models with  $t_{\text{duty}} = 0.5$  Gyr and  $r = 0$  (blue), 0.5 (orange), and 0.99 (green). In each panel we vary the initial  $\sigma_{M_*|M_h=10^{12}M_\odot}$  at  $z = 1$ ,  $\sigma_{M_*|M_h}^{\text{init}} = 0.2$ , 0.35, and 0.45 dex (left, center, and right panels, respectively).  $\sigma_{M_*|M_h}^{\text{init}} = 0.35$  and 0.45 dex are motivated by  $\sigma_{M_*|M_h}$  at  $M_h = 10^{12}$  and  $10^{11.5}M_\odot$ , respectively, in the Illustris TNG (Cao et al in preparation). The width of the shaded region represent the 68% confidence interval. We mark  $\sigma_{M_*|M_h}^{\text{init}}$  in black dashed. Increasing  $\sigma_{M_*|M_h}^{\text{init}}$ , increases  $\sigma_{M_*|M_h=10^{12}M_\odot}$  overall. However, for all  $\sigma_{M_*|M_h}^{\text{init}}$ ,  $r > 0$  reduces the  $\sigma_{M_*|M_h=10^{12}M_\odot}$  evolution. For the  $\sigma_{M_*|M_h}^{\text{init}} > 0.2$  dex models, even without galaxy assembly bias ( $r = 0$ ),  $t_{\text{duty}} = 0.5$  Gyr alone significantly tightens  $\sigma_{M_*|M_h=10^{12}M_\odot}$  from  $z = 1$  to 0 (blue). This is enhanced with  $r > 0$ . With  $r \geq 0.5$ , the  $\sigma_{M_*|M_h}^{\text{init}} > 0.2$  dex models can produce  $\sigma_{M_*|M_h=10^{12}M_\odot}$  evolutions consistent with the  $\sim 0.15$  dex decline in  $\sigma_{M_*|M_h=10^{12}M_\odot}$  Cao et al. (in preparation) find in Illustris TNG.

Component Analysis of the SFHs. However, it is consistent with the timescales found in the FIRE simulations (Hopkins et al. 2014; Sparre et al. 2017).

We examine the evolutionary trend of  $\sigma_{M_*|M_h=10^{12}M_\odot}$  in Figure 9, where we plot  $\sigma_{M_*|M_h=10^{12}M_\odot}$  from  $z = 1$  to 0 for our model with  $t_{\text{duty}} = 0.5$  Gyr and  $r = 0$  (blue), 0.5 (orange), and 0.99 (green). The width of the shaded region represent the 68% confidence interval. We mark the initial  $\sigma_{M_*|M_h=10^{12}M_\odot}$ ,  $\sigma_{M_*|M_h}^{\text{init}}$ , in black dashed;  $\sigma_{M_*|M_h}^{\text{init}} = 0.2$ , 0.35, and 0.45 dex in the left, center, and right panels, respectively. Focusing on the  $\sigma_{M_*|M_h}^{\text{init}} = 0.2$  panel (left), we find that for  $r > 0$  reduces the growth in  $\sigma_{M_*|M_h=10^{12}M_\odot}$  from  $\sigma_{M_*|M_h}^{\text{init}}$ . In fact, for  $r = 0.99$ , our model (green) predicts  $\sigma_{M_*|M_h=10^{12}M_\odot}$  that decreases from  $z = 1$ . For  $r \sim 0.6$  (Behroozi et al. 2019; Tinker et al. 2018a), we find a slight growth in  $\sigma_{M_*|M_h=10^{12}M_\odot}$  from  $z = 1$ :  $\sim 0.02$  dex (Figures 8 and 9). This is loosely consistent with halo model observations that find constant  $\sigma_{M_*|M_h} = 0.2$  dex evolution. However, as we discuss in Section 3.4, the constant  $\sigma_{M_*|M_h} = 0.2$  dex evolution from halo model observations is based on  $\sigma_{M_*|M_h}^{\text{init}} = 0.2$  dex constraints in the literature, which do not accurately reflect the SHMR scatter at  $z \sim 1$  at  $M_h = 10^{12}M_\odot$ .

Relaxing the  $\sigma_{M_*|M_h}^{\text{init}} = 0.2$  dex assumption, we present the  $\sigma_{M_*|M_h=10^{12}M_\odot}$  evolution for our models with  $\sigma_{M_*|M_h}^{\text{init}} = 0.35$  and 0.45 dex (center and right panels of Figure 9).  $\sigma_{M_*|M_h}^{\text{init}} = 0.35$  and 0.45 dex is motivated by  $\sigma_{M_*|M_h}$  at  $M_h = 10^{12}$  and  $10^{11.5}M_\odot$ , respectively, in Illustris TNG (Cao et al

in preparation). Increasing  $\sigma_{M_*|M_h}^{\text{init}}$ , increases  $\sigma_{M_*|M_h=10^{12}M_\odot}$  overall for all  $r$ . However, both a shorter  $t_{\text{duty}}$  and higher  $r$  produce tighter  $\sigma_{M_*|M_h=10^{12}M_\odot}$  in our  $\sigma_{M_*|M_h}^{\text{init}} > 0.2$  dex models. Hence,  $\sigma_{M_*|M_h=10^{12}M_\odot}$  remains sensitive to  $t_{\text{duty}}$  and  $r$ , regardless of  $\sigma_{M_*|M_h}^{\text{init}}$ . Figure 9 illustrates that for the  $\sigma_{M_*|M_h}^{\text{init}} > 0.2$  dex models, even without galaxy assembly bias ( $r = 0$ ),  $t_{\text{duty}} = 0.1$  Gyr alone significantly tightens  $\sigma_{M_*|M_h=10^{12}M_\odot}$  from  $z = 1$  to 0 (blue):  $\sim 0.06$  and  $0.11$  dex for  $\sigma_{M_*|M_h}^{\text{init}} = 0.35$  and  $0.45$  dex, respectively. With  $r > 0$ , the decline in  $\sigma_{M_*|M_h=10^{12}M_\odot}$  from  $z = 1$  to 0 is further enhanced. With  $r \geq 0.5$ , the  $\sigma_{M_*|M_h}^{\text{init}} > 0.2$  dex models can produce  $\sigma_{M_*|M_h=10^{12}M_\odot}$  evolutions consistent with the  $\sigma_{M_*|M_h=10^{12}M_\odot}$  decline Cao et al. (in preparation) find in the Illustris TNG.

In this section, we use our models with different  $t_{\text{duty}}$ ,  $r$ , and  $\sigma_{M_*|M_h}^{\text{init}}$  to investigate how these parameters impact predictions of  $\sigma_{M_*|M_h=10^{12}M_\odot}$  at  $z=0$ . A shorter timescale of star formation variability,  $t_{\text{duty}}$ , produces a tighter SHMR scatter. Higher correlation between SFH and halo assembly history, higher  $r$ , also produces a tighter SHMR scatter. Furthermore,  $\sigma_{M_*|M_h=10^{12}M_\odot}$  remains sensitive to  $t_{\text{duty}}$  and  $r$ , regardless of  $\sigma_{M_*|M_h}^{\text{init}}$ . Comparing our model predictions to  $\sigma_{M_*|M_h=10^{12}M_\odot}$  constraints in the literature, we find that by varying  $t_{\text{duty}}$  and  $r$  our model can produce  $\sigma_{M_*|M_h=10^{12}M_\odot}$  loosely consistent with constraints from observations and modern galaxy formation models, which span  $0.2 - 0.35$  dex. To reproduce the constant  $\sigma_{M_*|M_h} \sim 0.2$  dex evolution from  $z = 1$  to 0 found in halo model based observational constraints, our models require  $t_{\text{duty}} \leq 1.5$  Gyr for  $r = 0.99$  and  $r > 0.6$  for  $t_{\text{duty}} = 0.1$  Gyr. If we fix  $r = 0.6$ , the constraint on galaxy assembly bias from the literature,  $t_{\text{duty}} < 0.2$  Gyr is necessary. Meanwhile, to reproduce the  $\sigma_{M_*|M_h=10^{12}M_\odot} \sim 0.35$  to  $0.2$  dex decline from  $z = 1$  to 0 found in Illustris TNG, our models with  $\sigma_{M_*|M_h}^{\text{init}} > 0.2$  dex require  $r > 0.5$  for  $t_{\text{duty}} = 0.1$  Gyr. The lack of consensus among observations and galaxy formation models prevents us from precisely constraining  $t_{\text{duty}}$  or  $r$ . However, we illustrate that  $\sigma_{M_*|M_h=10^{12}M_\odot}$ , the scatter of the SHMR, is sensitive to  $t_{\text{duty}}$  and  $r$  and, thus, demonstrate that measurements of the SHMR relation can be used to constrain the detailed star formation histories of SF central galaxies and their connection to host halo assembly histories.

## 5. SUMMARY AND CONCLUSION

Despite our progress in understanding how galaxies form and evolve in the  $\Lambda$ CDM hierarchical universe, our understanding of the detailed star formation histories of galaxies and their connection to host halo assembly histories have been limited. This is in part due to the challenges in directly measuring SFHs in both observations and galaxy formation models. Empirical models, with their flexible prescriptions have made significant progress in better quantifying the SFHs of galaxies. These models, however, have yet to examine and constrain the timescale of star formation variability, which has the potential to constrain physical processes involved in star formation and galaxy feedback models. In this paper, we therefore focus on measuring the timescale of star formation variability and the connection between star formation and host halo accretion histories of star-forming central galaxies.

We combine the cosmological  $N$ -body **TreePM** simulation with SFHs that evolve the SF central galaxies along the SFS and present models that tracks the SFR,  $M_*$ , and host halo accretion histories of SF centrals from  $z \sim 1$  to  $z = 0.05$ . More specifically, we characterize the SFHs to evolve with respect to the mean log SFR of the SFS and introduce star formation variability using a “star formation

duty cycle”, where the SFRs of the SF centrals fluctuate about  $\log \text{SFR}_{\text{SFS}}$  on some timescale,  $t_{\text{duty}}$ . We parameterize the SFS using parameters that dictate the low  $M_*$  and high  $M_*$  slopes and redshift evolution. We then compare this model to the observed SMF of the SF centrals in the SDSS DR7 group catalog using ABC-PMC likelihood-free inference framework. When we examine the SHMR predicted by the model and inferred parameters we find:

- A shorter star formation duty cycle in our model produces significantly tighter scatter in the SHMR at  $M_h = 10^{12} M_\odot$ ,  $\sigma_{M_*|M_h=10^{12} M_\odot}$ . For  $t_{\text{duty}}$  from 10 to 0.1 Gyr, our model predicts  $\sigma_{M_*|M_h=10^{12} M_\odot} = 0.32^{+0.019}_{-0.021}$  to  $0.26^{+0.008}_{-0.008}$ . The dependence of  $\sigma_{M_*|M_h}$  on  $t_{\text{duty}}$  demonstrates that the scatter in SHMR can be used to constrain  $t_{\text{duty}}$ , and thus the timescale of star formation variability.
- We compare the  $\sigma_{M_*|M_h=10^{12} M_\odot}$  predicted by our model to observed constraints from halo occupation modeling of galaxy clustering, SMF, satellite kinematics, and galaxy-galaxy weak lensing. There is significant tension among the observational constraints and also among predictions from galaxy formation models with  $\sigma_{M_*|M_h=10^{12} M_\odot}$  spanning 0.2 to 0.35 dex. Among the literature, constraints from halo model based observations and hydrodynamic simulations find  $\sigma_{M_*|M_h=10^{12} M_\odot} \sim 0.2$  dex, which our model struggles to produce even with the shortest timescale we probe,  $t_{\text{duty}} = 0.1$  Gyr.
- We next examine models with assembly bias that correlate SFHs to host halo accretion histories with correlation coefficient,  $r$ . With stronger correlation, higher  $r$ , our models predict tighter scatter in the SHMR down to  $\sigma_{M_*|M_h=10^{12} M_\odot} = 0.17$  for  $r = 0.99$ . To produce  $\sigma_{M_*|M_h=10^{12} M_\odot} \sim 0.2$  dex, our models require  $r > 0.6$  for  $t_{\text{duty}} = 0.1$  Gyr or  $t_{\text{duty}} < 2$  Gyr for  $r = 0.99$ . For  $r \sim 0.6$ , as found in the literature,  $t_{\text{duty}} \lesssim 0.2$  Gyr is necessary. If we allow  $\sigma_{M_*|M_h}^{\text{init}}$  at  $z = 1$  to vary  $> 0.2$  dex, we find that our model requires  $r > 0.5$  for  $t_{\text{duty}} = 0.1$  Gyr to reproduce the  $\sigma_{M_*|M_h=10^{12} M_\odot} = 0.35$  to 0.2 dex evolution from  $z = 1$  to 0 in Illustris TNG.

Our work demonstrates that constraints on the scatter in the SHMR can be used to constrain both the timescale of star formation variability and the correlation between SFH and halo accretion history. The main bottleneck in deriving precise constraints remains the lack of consensus among  $\sigma_{M_*|M_h=10^{12} M_\odot}$  observations both at  $z = 0$  and 1. Also, while we focus on  $\sigma_{M_*|M_h}$  at  $M_h = 10^{12} M_\odot$ , the limit of current observations,  $\sigma_{M_*|M_h}$  is an even more sensitive probe at lower  $M_h$ . Upcoming surveys, however, will make significant progress on these fronts.

The Bright Galaxy Survey of the Dark Energy Spectroscopic Instrument (DESI; [Collaboration et al. 2016](#)), for instance, will observe  $\sim 10$  million galaxies down to the magnitude limit  $r \sim 20$  out to  $z \sim 0.5$ . This will enable BGS to more precisely constrain  $\sigma_{M_*|M_h}$  and resolve current tensions in observations at  $z = 0$ . Meanwhile, the Galaxy Evolution Survey of the Prime Focus Spectrograph ([Takada et al. 2014](#); [Tamura et al. 2016](#)), which will observe  $\sim 500,000$  galaxies between  $0.5 < z < 2.0$ , and the Wide-Area VISTA Extragalactic Survey (WAVES; [Driver et al. 2016, 2019](#)), which will observe  $\sim 2$  million galaxies down to  $r_{\text{AB}} < 22$  mag out to  $z \sim 1$ , will enable precise constraints of  $\sigma_{M_*|M_h}$  at  $z \sim 1$ . Using measurements from these surveys, our model will be able to

constrain the physical processes that govern star formation in galaxies and the detailed connection between star formation and host halo accretion.

#### ACKNOWLEDGEMENTS

It's a pleasure to thank J.D. Cohn, Shirley Ho, and Tjitske Starkenburg for valuable discussions and feedback. We also thank Louis E. Abramson, Junzhi Cao, Shy Genel, and Cheng Li for providing us with data used in the analysis. This material is based upon work supported by the U.S. Department of Energy, Office of Science, Office of High Energy Physics, under contract No. DE-AC02-05CH11231. AW was supported by NASA, through ATP grant 80NSSC18K1097 and HST grants GO-14734 and AR-15057 from STScI.

#### REFERENCES

- Abazajian, K. N., Adelman-McCarthy, J. K., Agüeros, M. A., et al. 2009, *The Astrophysical Journal Supplement Series*, 182, 543, doi: [10.1088/0067-0049/182/2/543](https://doi.org/10.1088/0067-0049/182/2/543)
- Abramson, L. E., Gladders, M. D., Dressler, A., et al. 2016, *The Astrophysical Journal*, 832, 7, doi: [10.3847/0004-637X/832/1/7](https://doi.org/10.3847/0004-637X/832/1/7)
- . 2015, *The Astrophysical Journal Letters*, 801, L12, doi: [10.1088/2041-8205/801/1/L12](https://doi.org/10.1088/2041-8205/801/1/L12)
- Alsing, J., Wandelt, B., & Feeney, S. 2018, arXiv:1801.01497 [astro-ph]. <https://arxiv.org/abs/1801.01497>
- Artale, M. C., Zehavi, I., Contreras, S., & Norberg, P. 2018, *Monthly Notices of the Royal Astronomical Society*, 480, 3978, doi: [10.1093/mnras/sty2110](https://doi.org/10.1093/mnras/sty2110)
- Baldry, I. K., Balogh, M. L., Bower, R. G., et al. 2006, *Monthly Notices of the Royal Astronomical Society*, 373, 469, doi: [10.1111/j.1365-2966.2006.11081.x](https://doi.org/10.1111/j.1365-2966.2006.11081.x)
- Becker, M. R. 2015, arXiv e-prints, 1507, arXiv:1507.03605
- Behroozi, P., Wechsler, R. H., Hearin, A. P., & Conroy, C. 2019, *Monthly Notices of the Royal Astronomical Society*, 1134, doi: [10.1093/mnras/stz1182](https://doi.org/10.1093/mnras/stz1182)
- Behroozi, P. S., Wechsler, R. H., & Conroy, C. 2013, *The Astrophysical Journal*, 770, 57, doi: [10.1088/0004-637X/770/1/57](https://doi.org/10.1088/0004-637X/770/1/57)
- Bekki, K. 2009, *Monthly Notices of the Royal Astronomical Society*, 399, 2221, doi: [10.1111/j.1365-2966.2009.15431.x](https://doi.org/10.1111/j.1365-2966.2009.15431.x)
- Blanton, M. R. 2006, *The Astrophysical Journal*, 648, 268, doi: [10.1086/505628](https://doi.org/10.1086/505628)
- Blanton, M. R., & Moustakas, J. 2009, *Annual Review of Astronomy and Astrophysics*, 47, 159, doi: [10.1146/annurev-astro-082708-101734](https://doi.org/10.1146/annurev-astro-082708-101734)
- Blanton, M. R., & Roweis, S. 2007, *The Astronomical Journal*, 133, 734, doi: [10.1086/510127](https://doi.org/10.1086/510127)
- Blanton, M. R., Hogg, D. W., Bahcall, N. A., et al. 2003, *The Astrophysical Journal*, 594, 186, doi: [10.1086/375528](https://doi.org/10.1086/375528)
- Blanton, M. R., Schlegel, D. J., Strauss, M. A., et al. 2005, *The Astronomical Journal*, 129, 2562, doi: [10.1086/429803](https://doi.org/10.1086/429803)
- Borch, A., Meisenheimer, K., Bell, E. F., et al. 2006, *Astronomy and Astrophysics*, 453, 869, doi: [10.1051/0004-6361:20054376](https://doi.org/10.1051/0004-6361:20054376)
- Brinchmann, J., Charlot, S., White, S. D. M., et al. 2004, *Monthly Notices of the Royal Astronomical Society*, 351, 1151, doi: [10.1111/j.1365-2966.2004.07881.x](https://doi.org/10.1111/j.1365-2966.2004.07881.x)
- Bundy, K., Ellis, R. S., Conselice, C. J., et al. 2006, *The Astrophysical Journal*, 651, 120, doi: [10.1086/507456](https://doi.org/10.1086/507456)
- Calderon, V. F., Berlind, A. A., & Sinha, M. 2018, *Monthly Notices of the Royal Astronomical Society*, 480, 2031, doi: [10.1093/mnras/sty2000](https://doi.org/10.1093/mnras/sty2000)
- Cameron, E., & Pettitt, A. N. 2012, *Monthly Notices of the Royal Astronomical Society*, 425, 44, doi: [10.1111/j.1365-2966.2012.21371.x](https://doi.org/10.1111/j.1365-2966.2012.21371.x)
- Campbell, D., van den Bosch, F. C., Hearin, A., et al. 2015, *Monthly Notices of the Royal Astronomical Society*, 452, 444, doi: [10.1093/mnras/stv1091](https://doi.org/10.1093/mnras/stv1091)

- Carnall, A. C., Leja, J., Johnson, B. D., et al. 2018, arXiv:1811.03635 [astro-ph].  
<https://arxiv.org/abs/1811.03635>
- Chabrier, G. 2003, Publications of the Astronomical Society of the Pacific, 115, 763, doi: [10.1086/376392](https://doi.org/10.1086/376392)
- Cohn, J. D. 2017, Monthly Notices of the Royal Astronomical Society, 466, 2718, doi: [10.1093/mnras/stw3202](https://doi.org/10.1093/mnras/stw3202)
- Collaboration, D., Aghamousa, A., Aguilar, J., et al. 2016, arXiv:1611.00036 [astro-ph].  
<https://arxiv.org/abs/1611.00036>
- Conroy, C., Gunn, J. E., & White, M. 2009, The Astrophysical Journal, 699, 486, doi: [10.1088/0004-637X/699/1/486](https://doi.org/10.1088/0004-637X/699/1/486)
- Conroy, C., Wechsler, R. H., & Kravtsov, A. V. 2006, The Astrophysical Journal, 647, 201, doi: [10.1086/503602](https://doi.org/10.1086/503602)
- Conroy, C., Prada, F., Newman, J. A., et al. 2007, The Astrophysical Journal, 654, 153, doi: [10.1086/509632](https://doi.org/10.1086/509632)
- Croton, D. J., Gao, L., & White, S. D. M. 2007, Monthly Notices of the Royal Astronomical Society, 374, 1303, doi: [10.1111/j.1365-2966.2006.11230.x](https://doi.org/10.1111/j.1365-2966.2006.11230.x)
- Croton, D. J., Stevens, A. R. H., Tonini, C., et al. 2016, The Astrophysical Journal Supplement Series, 222, 22, doi: [10.3847/0067-0049/222/2/22](https://doi.org/10.3847/0067-0049/222/2/22)
- Daddi, E., Dickinson, M., Morrison, G., et al. 2007, The Astrophysical Journal, 670, 156, doi: [10.1086/521818](https://doi.org/10.1086/521818)
- Davis, M., Efstathiou, G., Frenk, C. S., & White, S. D. M. 1985, The Astrophysical Journal, 292, 371, doi: [10.1086/163168](https://doi.org/10.1086/163168)
- Dawson, K. S., Schlegel, D. J., Ahn, C. P., et al. 2013, The Astronomical Journal, 145, 10, doi: [10.1088/0004-6256/145/1/10](https://doi.org/10.1088/0004-6256/145/1/10)
- Diemer, B., Sparre, M., Abramson, L. E., & Torrey, P. 2017, The Astrophysical Journal, 839, 26, doi: [10.3847/1538-4357/aa68e5](https://doi.org/10.3847/1538-4357/aa68e5)
- Driver, S. P., Davies, L. J., Meyer, M., et al. 2016, The Universe of Digital Sky Surveys, 42, 205, doi: [10.1007/978-3-319-19330-4\\_32](https://doi.org/10.1007/978-3-319-19330-4_32)
- Driver, S. P., Liske, J., Davies, L. J. M., et al. 2019, The Messenger, 175, 46, doi: [10.18727/0722-6691/5126](https://doi.org/10.18727/0722-6691/5126)
- Drory, N., Bundy, K., Leauthaud, A., et al. 2009, The Astrophysical Journal, 707, 1595, doi: [10.1088/0004-637X/707/2/1595](https://doi.org/10.1088/0004-637X/707/2/1595)
- Elbaz, D., Daddi, E., Le Borgne, D., et al. 2007, Astronomy and Astrophysics, 468, 33, doi: [10.1051/0004-6361:20077525](https://doi.org/10.1051/0004-6361:20077525)
- Gao, L., Springel, V., & White, S. D. M. 2005, Monthly Notices of the Royal Astronomical Society, 363, L66, doi: [10.1111/j.1745-3933.2005.00084.x](https://doi.org/10.1111/j.1745-3933.2005.00084.x)
- Gao, L., & White, S. D. M. 2007, Monthly Notices of the Royal Astronomical Society, 377, L5, doi: [10.1111/j.1745-3933.2007.00292.x](https://doi.org/10.1111/j.1745-3933.2007.00292.x)
- Genel, S., Vogelsberger, M., Springel, V., et al. 2014, Monthly Notices of the Royal Astronomical Society, 445, 175, doi: [10.1093/mnras/stu1654](https://doi.org/10.1093/mnras/stu1654)
- Gladders, M. D., Oemler, A., Dressler, A., et al. 2013, The Astrophysical Journal, 770, 64, doi: [10.1088/0004-637X/770/1/64](https://doi.org/10.1088/0004-637X/770/1/64)
- Governato, F., Weisz, D., Pontzen, A., et al. 2015, Monthly Notices of the Royal Astronomical Society, 448, 792, doi: [10.1093/mnras/stu2720](https://doi.org/10.1093/mnras/stu2720)
- Gu, M., Conroy, C., & Behroozi, P. 2016, The Astrophysical Journal, 833, 2, doi: [10.3847/0004-637X/833/1/2](https://doi.org/10.3847/0004-637X/833/1/2)
- Gunn, J. E., & Gott, III, J. R. 1972, The Astrophysical Journal, 176, 1, doi: [10.1086/151605](https://doi.org/10.1086/151605)
- Hahn, C., Beutler, F., Sinha, M., et al. 2018a, ArXiv e-prints, 1803, arXiv:1803.06348
- Hahn, C., Tinker, J. L., & Wetzel, A. R. 2017a, The Astrophysical Journal, 841, 6, doi: [10.3847/1538-4357/aa6d6b](https://doi.org/10.3847/1538-4357/aa6d6b)
- Hahn, C., Vakili, M., Walsh, K., et al. 2017b, Monthly Notices of the Royal Astronomical Society, 469, 2791, doi: [10.1093/mnras/stx894](https://doi.org/10.1093/mnras/stx894)
- Hahn, C., Blanton, M. R., Moustakas, J., et al. 2015, The Astrophysical Journal, 806, 162, doi: [10.1088/0004-637X/806/2/162](https://doi.org/10.1088/0004-637X/806/2/162)
- Hahn, C., Starkenburg, T. K., Choi, E., et al. 2018b
- Han, J., Eke, V. R., Frenk, C. S., et al. 2015, Monthly Notices of the Royal Astronomical Society, 446, 1356, doi: [10.1093/mnras/stu2178](https://doi.org/10.1093/mnras/stu2178)
- Hopkins, A. M., & Beacom, J. F. 2006, The Astrophysical Journal, 651, 142, doi: [10.1086/506610](https://doi.org/10.1086/506610)
- Hopkins, P. F., Kereš, D., Oñorbe, J., et al. 2014, Monthly Notices of the Royal Astronomical Society, 445, 581, doi: [10.1093/mnras/stu1738](https://doi.org/10.1093/mnras/stu1738)



- Illbert, O., McCracken, H. J., Le Fèvre, O., et al. 2013, *Astronomy and Astrophysics*, 556, A55, doi: [10.1051/0004-6361/201321100](https://doi.org/10.1051/0004-6361/201321100)
- Ishida, E. E. O., Vitenti, S. D. P., Penna-Lima, M., et al. 2015, *Astronomy and Computing*, 13, 1, doi: [10.1016/j.ascom.2015.09.001](https://doi.org/10.1016/j.ascom.2015.09.001)
- Karim, A., Schinnerer, E., Martínez-Sansigre, A., et al. 2011, *The Astrophysical Journal*, 730, 61, doi: [10.1088/0004-637X/730/2/61](https://doi.org/10.1088/0004-637X/730/2/61)
- Kauffmann, G., Heckman, T. M., White, S. D. M., et al. 2003, *Monthly Notices of the Royal Astronomical Society*, 341, 54, doi: [10.1046/j.1365-8711.2003.06292.x](https://doi.org/10.1046/j.1365-8711.2003.06292.x)
- Kelson, D. D. 2014, arXiv:1406.5191 [astro-ph]. <https://arxiv.org/abs/1406.5191>
- Khandai, N., Di Matteo, T., Croft, R., et al. 2015, *Monthly Notices of the Royal Astronomical Society*, 450, 1349, doi: [10.1093/mnras/stv627](https://doi.org/10.1093/mnras/stv627)
- Kravtsov, A. V., Berlind, A. A., Wechsler, R. H., et al. 2004, *The Astrophysical Journal*, 609, 35, doi: [10.1086/420959](https://doi.org/10.1086/420959)
- Lacerna, I., Padilla, N., & Stasyszyn, F. 2014, *Monthly Notices of the Royal Astronomical Society*, 443, 3107, doi: [10.1093/mnras/stu1318](https://doi.org/10.1093/mnras/stu1318)
- Lange, J. U., van den Bosch, F. C., Zentner, A. R., Wang, K., & Villarreal, A. S. 2018, arXiv:1811.03596 [astro-ph]. <https://arxiv.org/abs/1811.03596>
- Larson, R. B., Tinsley, B. M., & Caldwell, C. N. 1980, *The Astrophysical Journal*, 237, 692, doi: [10.1086/157917](https://doi.org/10.1086/157917)
- Leauthaud, A., Tinker, J., Bundy, K., et al. 2012, *The Astrophysical Journal*, 744, 159, doi: [10.1088/0004-637X/744/2/159](https://doi.org/10.1088/0004-637X/744/2/159)
- Lee, N., Sanders, D. B., Casey, C. M., et al. 2015, *The Astrophysical Journal*, 801, 80, doi: [10.1088/0004-637X/801/2/80](https://doi.org/10.1088/0004-637X/801/2/80)
- Leja, J., Carnall, A. C., Johnson, B. D., Conroy, C., & Speagle, J. S. 2018, arXiv:1811.03637 [astro-ph]. <https://arxiv.org/abs/1811.03637>
- Leja, J., van Dokkum, P., & Franx, M. 2013, *The Astrophysical Journal*, 766, doi: [10.1088/0004-637X/766/1/33](https://doi.org/10.1088/0004-637X/766/1/33)
- Leja, J., van Dokkum, P. G., Franx, M., & Whitaker, K. E. 2015, 798, 115, doi: [10.1088/0004-637X/798/2/115](https://doi.org/10.1088/0004-637X/798/2/115)
- Li, C., & White, S. D. M. 2009, *Monthly Notices of the Royal Astronomical Society*, 398, 2177, doi: [10.1111/j.1365-2966.2009.15268.x](https://doi.org/10.1111/j.1365-2966.2009.15268.x)
- Li, Y., Mo, H. J., & Gao, L. 2008, *Monthly Notices of the Royal Astronomical Society*, 389, 1419, doi: [10.1111/j.1365-2966.2008.13667.x](https://doi.org/10.1111/j.1365-2966.2008.13667.x)
- Lim, S. H., Mo, H. J., Wang, H., & Yang, X. 2016, *Monthly Notices of the Royal Astronomical Society*, 455, 499, doi: [10.1093/mnras/stv2282](https://doi.org/10.1093/mnras/stv2282)
- Lu, Y., Wechsler, R. H., Somerville, R. S., et al. 2014, *The Astrophysical Journal*, 795, 123, doi: [10.1088/0004-637X/795/2/123](https://doi.org/10.1088/0004-637X/795/2/123)
- Madau, P., & Dickinson, M. 2014, *Annual Review of Astronomy and Astrophysics*, 52, 415, doi: [10.1146/annurev-astro-081811-125615](https://doi.org/10.1146/annurev-astro-081811-125615)
- Magdis, G. E., Daddi, E., Béthermin, M., et al. 2012, *The Astrophysical Journal*, 760, 6, doi: [10.1088/0004-637X/760/1/6](https://doi.org/10.1088/0004-637X/760/1/6)
- Mamon, G. A., Sanchis, T., Salvador-Solé, E., & Solanes, J. M. 2004, *Astronomy and Astrophysics*, 414, 445, doi: [10.1051/0004-6361:20034155](https://doi.org/10.1051/0004-6361:20034155)
- Mandelbaum, R., Seljak, U., Kauffmann, G., Hirata, C. M., & Brinkmann, J. 2006, *Monthly Notices of the Royal Astronomical Society*, 368, 715, doi: [10.1111/j.1365-2966.2006.10156.x](https://doi.org/10.1111/j.1365-2966.2006.10156.x)
- Marchesini, D., van Dokkum, P. G., Förster Schreiber, N. M., et al. 2009, *The Astrophysical Journal*, 701, 1765, doi: [10.1088/0004-637X/701/2/1765](https://doi.org/10.1088/0004-637X/701/2/1765)
- Matthee, J., Schaye, J., Crain, R. A., et al. 2017, *Monthly Notices of the Royal Astronomical Society*, 465, 2381, doi: [10.1093/mnras/stw2884](https://doi.org/10.1093/mnras/stw2884)
- Mitra, S., Davé, R., & Finlator, K. 2015, *Monthly Notices of the Royal Astronomical Society*, 452, 1184, doi: [10.1093/mnras/stv1387](https://doi.org/10.1093/mnras/stv1387)
- Mitra, S., Davé, R., Simha, V., & Finlator, K. 2017, *Monthly Notices of the Royal Astronomical Society*, 464, 2766, doi: [10.1093/mnras/stw2527](https://doi.org/10.1093/mnras/stw2527)
- Moore, B., Lake, G., & Katz, N. 1998, *The Astrophysical Journal*, 495, 139, doi: [10.1086/305264](https://doi.org/10.1086/305264)
- More, S., van den Bosch, F. C., Cacciato, M., et al. 2011, *Monthly Notices of the Royal Astronomical Society*, 410, 210, doi: [10.1111/j.1365-2966.2010.17436.x](https://doi.org/10.1111/j.1365-2966.2010.17436.x)
- Moster, B. P., Naab, T., & White, S. D. M. 2013, *Monthly Notices of the Royal Astronomical Society*, 428, 3121, doi: [10.1093/mnras/sts261](https://doi.org/10.1093/mnras/sts261)
- . 2017, arXiv:1705.05373 [astro-ph]. <https://arxiv.org/abs/1705.05373>

- Moustakas, J., Coil, A. L., Aird, J., et al. 2013, *The Astrophysical Journal*, 767, 50, doi: [10.1088/0004-637X/767/1/50](https://doi.org/10.1088/0004-637X/767/1/50)
- Muzzin, A., Marchesini, D., Stefanon, M., et al. 2013, *The Astrophysical Journal*, 777, 18, doi: [10.1088/0004-637X/777/1/18](https://doi.org/10.1088/0004-637X/777/1/18)
- Noeske, K. G., Weiner, B. J., Faber, S. M., et al. 2007, *The Astrophysical Journal Letters*, 660, L43, doi: [10.1086/517926](https://doi.org/10.1086/517926)
- Parejko, J. K., Sunayama, T., Padmanabhan, N., et al. 2013, *Monthly Notices of the Royal Astronomical Society*, 429, 98, doi: [10.1093/mnras/sts314](https://doi.org/10.1093/mnras/sts314)
- Patel, S. G., Kelson, D. D., Williams, R. J., et al. 2015, *The Astrophysical Journal Letters*, 799, L17, doi: [10.1088/2041-8205/799/2/L17](https://doi.org/10.1088/2041-8205/799/2/L17)
- Peng, Y., Maiolino, R., & Cochrane, R. 2015, *Nature*, 521, 192, doi: [10.1038/nature14439](https://doi.org/10.1038/nature14439)
- Peng, Y.-j., Lilly, S. J., Kovač, K., et al. 2010, *The Astrophysical Journal*, 721, 193, doi: [10.1088/0004-637X/721/1/193](https://doi.org/10.1088/0004-637X/721/1/193)
- Pillepich, A., Springel, V., Nelson, D., et al. 2018, *Monthly Notices of the Royal Astronomical Society*, 473, 4077, doi: [10.1093/mnras/stx2656](https://doi.org/10.1093/mnras/stx2656)
- Reddick, R. M., Wechsler, R. H., Tinker, J. L., & Behroozi, P. S. 2013, *The Astrophysical Journal*, 771, 30, doi: [10.1088/0004-637X/771/1/30](https://doi.org/10.1088/0004-637X/771/1/30)
- Rodríguez-Puebla, A., Primack, J. R., Behroozi, P., & Faber, S. M. 2016, *Monthly Notices of the Royal Astronomical Society*, 455, 2592, doi: [10.1093/mnras/stv2513](https://doi.org/10.1093/mnras/stv2513)
- Roediger, J. C., & Courteau, S. 2015, *Monthly Notices of the Royal Astronomical Society*, 452, 3209, doi: [10.1093/mnras/stv1499](https://doi.org/10.1093/mnras/stv1499)
- Salim, S., Rich, R. M., Charlot, S., et al. 2007, *The Astrophysical Journal Supplement Series*, 173, 267, doi: [10.1086/519218](https://doi.org/10.1086/519218)
- Santini, P., Fontana, A., Grazian, A., et al. 2009, *Astronomy and Astrophysics*, 504, 751, doi: [10.1051/0004-6361/200811434](https://doi.org/10.1051/0004-6361/200811434)
- Schreiber, C., Pannella, M., Elbaz, D., et al. 2015, *Astronomy and Astrophysics*, 575, A74, doi: [10.1051/0004-6361/201425017](https://doi.org/10.1051/0004-6361/201425017)
- Silk, J., & Mamon, G. A. 2012, *Research in Astronomy and Astrophysics*, 12, 917, doi: [10.1088/1674-4527/12/8/004](https://doi.org/10.1088/1674-4527/12/8/004)
- Somerville, R. S., & Davé, R. 2015, *Annual Review of Astronomy and Astrophysics*, 53, 51, doi: [10.1146/annurev-astro-082812-140951](https://doi.org/10.1146/annurev-astro-082812-140951)
- Somerville, R. S., Gilmore, R. C., Primack, J. R., & Domínguez, A. 2012, *Monthly Notices of the Royal Astronomical Society*, 423, 1992, doi: [10.1111/j.1365-2966.2012.20490.x](https://doi.org/10.1111/j.1365-2966.2012.20490.x)
- Sparre, M., Hayward, C. C., Feldmann, R., et al. 2017, *Monthly Notices of the Royal Astronomical Society*, 466, 88, doi: [10.1093/mnras/stw3011](https://doi.org/10.1093/mnras/stw3011)
- Sparre, M., Hayward, C. C., Springel, V., et al. 2015, *Monthly Notices of the Royal Astronomical Society*, 447, 3548, doi: [10.1093/mnras/stu2713](https://doi.org/10.1093/mnras/stu2713)
- Speagle, J. S., Steinhardt, C. L., Capak, P. L., & Silverman, J. D. 2014, *The Astrophysical Journal Supplement Series*, 214, 15, doi: [10.1088/0067-0049/214/2/15](https://doi.org/10.1088/0067-0049/214/2/15)
- Sunayama, T., Hearin, A. P., Padmanabhan, N., & Leauthaud, A. 2016, *Monthly Notices of the Royal Astronomical Society*, 458, 1510, doi: [10.1093/mnras/stw332](https://doi.org/10.1093/mnras/stw332)
- Taghizadeh-Popp, M., Fall, S. M., White, R. L., & Szalay, A. S. 2015, *The Astrophysical Journal*, 801, 14, doi: [10.1088/0004-637X/801/1/14](https://doi.org/10.1088/0004-637X/801/1/14)
- Takada, M., Ellis, R. S., Chiba, M., et al. 2014, *Publications of the Astronomical Society of Japan*, 66, R1, doi: [10.1093/pasj/pst019](https://doi.org/10.1093/pasj/pst019)
- Tamura, N., Takato, N., Shimono, A., et al. 2016, in *Ground-Based and Airborne Instrumentation for Astronomy VI*, Vol. 9908, eprint: arXiv:1608.01075, 99081M
- Taylor, E. N., Franx, M., van Dokkum, P. G., et al. 2009, *The Astrophysical Journal*, 694, 1171, doi: [10.1088/0004-637X/694/2/1171](https://doi.org/10.1088/0004-637X/694/2/1171)
- Tinker, J., Wetzel, A., & Conroy, C. 2011, *ArXiv e-prints*, 1107, arXiv:1107.5046
- Tinker, J. L., Hahn, C., Mao, Y.-Y., & Wetzel, A. R. 2018a, *Monthly Notices of the Royal Astronomical Society*, 478, 4487, doi: [10.1093/mnras/sty1263](https://doi.org/10.1093/mnras/sty1263)
- Tinker, J. L., Hahn, C., Mao, Y.-Y., Wetzel, A. R., & Conroy, C. 2018b, *Monthly Notices of the Royal Astronomical Society*, 477, 935, doi: [10.1093/mnras/sty666](https://doi.org/10.1093/mnras/sty666)
- Tinker, J. L., Leauthaud, A., Bundy, K., et al. 2013, *The Astrophysical Journal*, 778, 93, doi: [10.1088/0004-637X/778/2/93](https://doi.org/10.1088/0004-637X/778/2/93)
- Tinker, J. L., Wetzel, A. R., Conroy, C., & Mao, Y.-Y. 2017a, *Monthly Notices of the Royal Astronomical Society*, 472, 2504, doi: [10.1093/mnras/stx2066](https://doi.org/10.1093/mnras/stx2066)

- Tinker, J. L., Brownstein, J. R., Guo, H., et al. 2017b, *The Astrophysical Journal*, 839, 121, doi: [10.3847/1538-4357/aa6845](https://doi.org/10.3847/1538-4357/aa6845)
- Tojeiro, R., Wilkins, S., Heavens, A. F., Panter, B., & Jimenez, R. 2009, *The Astrophysical Journal Supplement Series*, 185, 1, doi: [10.1088/0067-0049/185/1/1](https://doi.org/10.1088/0067-0049/185/1/1)
- Tojeiro, R., Eardley, E., Peacock, J. A., et al. 2017, *Monthly Notices of the Royal Astronomical Society*, 470, 3720, doi: [10.1093/mnras/stx1466](https://doi.org/10.1093/mnras/stx1466)
- Vale, A., & Ostriker, J. P. 2006, *Monthly Notices of the Royal Astronomical Society*, 371, 1173, doi: [10.1111/j.1365-2966.2006.10605.x](https://doi.org/10.1111/j.1365-2966.2006.10605.x)
- Velander, M., van Uitert, E., Hoekstra, H., et al. 2014, *Monthly Notices of the Royal Astronomical Society*, 437, 2111, doi: [10.1093/mnras/stt2013](https://doi.org/10.1093/mnras/stt2013)
- Vogelsberger, M., Genel, S., Springel, V., et al. 2014, *Monthly Notices of the Royal Astronomical Society*, 444, 1518, doi: [10.1093/mnras/stu1536](https://doi.org/10.1093/mnras/stu1536)
- Wang, L., Farrah, D., Oliver, S. J., et al. 2013, *Monthly Notices of the Royal Astronomical Society*, 431, 648, doi: [10.1093/mnras/stt190](https://doi.org/10.1093/mnras/stt190)
- Wang, Y., Yang, X., Mo, H. J., et al. 2008, *The Astrophysical Journal*, 687, 919, doi: [10.1086/591836](https://doi.org/10.1086/591836)
- Wechsler, R. H., & Tinker, J. L. 2018, ArXiv e-prints, 1804, arXiv:1804.03097
- Wechsler, R. H., Zentner, A. R., Bullock, J. S., Kravtsov, A. V., & Allgood, B. 2006, *The Astrophysical Journal*, 652, 71, doi: [10.1086/507120](https://doi.org/10.1086/507120)
- Wetzel, A. R., Cohn, J. D., & White, M. 2009, *Monthly Notices of the Royal Astronomical Society*, 395, 1376, doi: [10.1111/j.1365-2966.2009.14424.x](https://doi.org/10.1111/j.1365-2966.2009.14424.x)
- Wetzel, A. R., Cohn, J. D., White, M., Holz, D. E., & Warren, M. S. 2007, *The Astrophysical Journal*, 656, 139, doi: [10.1086/510444](https://doi.org/10.1086/510444)
- Wetzel, A. R., Tinker, J. L., & Conroy, C. 2012, *Monthly Notices of the Royal Astronomical Society*, 424, 232, doi: [10.1111/j.1365-2966.2012.21188.x](https://doi.org/10.1111/j.1365-2966.2012.21188.x)
- Wetzel, A. R., Tinker, J. L., Conroy, C., & van den Bosch, F. C. 2013, *Monthly Notices of the Royal Astronomical Society*, 432, 336, doi: [10.1093/mnras/stt469](https://doi.org/10.1093/mnras/stt469)
- . 2014, *Monthly Notices of the Royal Astronomical Society*, 439, 2687, doi: [10.1093/mnras/stu122](https://doi.org/10.1093/mnras/stu122)
- Wetzel, A. R., & White, M. 2010, *Monthly Notices of the Royal Astronomical Society*, 403, 1072, doi: [10.1111/j.1365-2966.2009.16191.x](https://doi.org/10.1111/j.1365-2966.2009.16191.x)
- Weyant, A., Schafer, C., & Wood-Vasey, W. M. 2013, *The Astrophysical Journal*, 764, 116, doi: [10.1088/0004-637X/764/2/116](https://doi.org/10.1088/0004-637X/764/2/116)
- Whitaker, K. E., van Dokkum, P. G., Brammer, G., & Franx, M. 2012, *The Astrophysical Journal Letters*, 754, L29, doi: [10.1088/2041-8205/754/2/L29](https://doi.org/10.1088/2041-8205/754/2/L29)
- White, M. 2002, *The Astrophysical Journal Supplement Series*, 143, 241, doi: [10.1086/342752](https://doi.org/10.1086/342752)
- White, M., Cohn, J. D., & Smit, R. 2010, *Monthly Notices of the Royal Astronomical Society*, 408, 1818, doi: [10.1111/j.1365-2966.2010.17248.x](https://doi.org/10.1111/j.1365-2966.2010.17248.x)
- Wilkinson, D. M., Maraston, C., Goddard, D., Thomas, D., & Parikh, T. 2017, arXiv:1711.00865 [astro-ph]. <https://arxiv.org/abs/1711.00865>
- Yang, X., Mo, H. J., & van den Bosch, F. C. 2006, *The Astrophysical Journal Letters*, 638, L55, doi: [10.1086/501069](https://doi.org/10.1086/501069)
- . 2009, *The Astrophysical Journal*, 695, 900, doi: [10.1088/0004-637X/695/2/900](https://doi.org/10.1088/0004-637X/695/2/900)
- Yang, X., Mo, H. J., van den Bosch, F. C., & Jing, Y. P. 2005, *Monthly Notices of the Royal Astronomical Society*, 356, 1293, doi: [10.1111/j.1365-2966.2005.08560.x](https://doi.org/10.1111/j.1365-2966.2005.08560.x)
- York, D. G., Adelman, J., Anderson, Jr., J. E., et al. 2000, *The Astronomical Journal*, 120, 1579, doi: [10.1086/301513](https://doi.org/10.1086/301513)
- Zehavi, I., Contreras, S., Padilla, N., et al. 2018, *The Astrophysical Journal*, 853, 84, doi: [10.3847/1538-4357/aaa54a](https://doi.org/10.3847/1538-4357/aaa54a)
- Zehavi, I., Zheng, Z., Weinberg, D. H., et al. 2011, *The Astrophysical Journal*, 736, 59, doi: [10.1088/0004-637X/736/1/59](https://doi.org/10.1088/0004-637X/736/1/59)
- Zheng, Z., Coil, A. L., & Zehavi, I. 2007, *The Astrophysical Journal*, 667, 760, doi: [10.1086/521074](https://doi.org/10.1086/521074)
- Zu, Y., & Mandelbaum, R. 2015, *Monthly Notices of the Royal Astronomical Society*, 454, 1161, doi: [10.1093/mnras/stv2062](https://doi.org/10.1093/mnras/stv2062)